CHALMERS
UNIVERSITY OF TECHNOLOGY

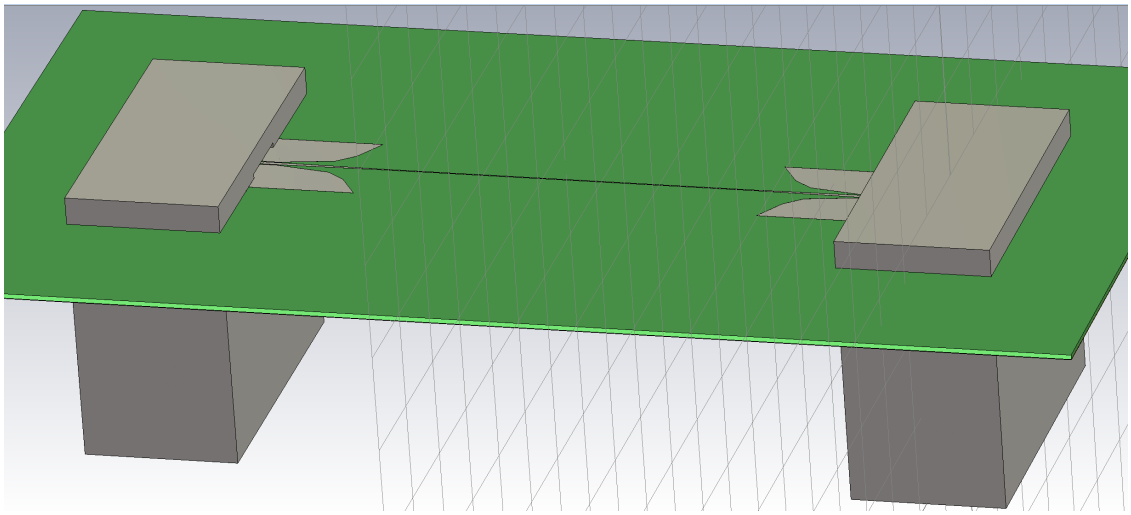

Design of a rectangular waveguide connected biosensor for frequencies from 220 to 1100 GHz

Master's thesis

PATRICIA NOVALBOS LAINA

Terahertz and Millimetre Wave Laboratory
Department of Microtechnology and Nanoscience (MC2)
CHALMERS UNIVERSITY OF TECHNOLOGY
Gothenburg, Sweden 2015

Master's thesis

Design of a rectangular waveguide connected biosensor for frequencies from 220 to 1100 GHz

PATRICIA NOVALBOS LAINA

Universidad Carlos III de Madrid

Department of Microtechnology and Nanoscience (MC2)
Chalmers University of Technology
Gothenburg, Sweden 2015

Design of a rectangular waveguide connected biosensor for frequencies from 220 to 1100 GHz
PATRICIA NOVALBOS LAINA

Supervisor: Helena Rodilla, Department of Microtechnology and Nanoscience (MC2)
Examiner: Josip Vukusic,Department of Microtechnology and Nanoscience (MC2)
Supervisor (UC3M): Jesús Arroyo Hernández, Departamento de Teoría de la Señal y Comunicaciones.

Department of Microtechnology and Nanoscience (MC2)
Terahertz and Millimetre Wave Laboratory
Chalmers University of Technology
SE-412 96 Gothenburg
Telephone +46 31 772 1000

Cover: Illustration of the transition presented in this thesis.

Typeset in LaTeX
Gothenburg, Sweden 2015

To my family

♡

Design of a rectangular waveguide based interchangeable biosensor at 2201100 GHz
PATRICIA NOVALBOS LAINA
Department of Microtechnology and Nanoscience (MC2)
Chalmers University of Technology

Abstract

Biomolecules have vibrational and rotational resonances at THz frequencies (0.1 to 10 THz) due to their structure and size. This unique interaction between electromagnetic waves in the THz frequency region and biological matter promises a multitude of applications of terahertz technology in life sciences, further enabled by the latest development of sources and detectors at this frequency range. Due to the emerging status of this new research field, there are many challenges to overcome when applying THz reflection and transmission measurements in biological samples. One of the challenges is the robustness and repeatability of the measurements.

In this work, a biosensor design based on a transition between a rectangular waveguide (WR3, WR2, WR1.5 and WR1) and a Planar Goubau line (PGL) is presented for four different frequency ranges, from 220 GHz to 1.1 THz. With the proposed design, we leave probes and positioners aside, connecting the rectangular waveguides directly to the VNA and alleviating the uncertainty problems of on-probe measurements.

Keywords: THz, life sciences, rectangular waveguides, PGL, CPW, uncertainty consequence of on-probe measurements, VNA, 220 GHz, 1.1 THz.

Resumen

En este Proyecto Fin de Carrera, realizado en Chalmers University of Technology, se ha diseñado un sensor basado en una transición entre una guía de onda rectangular (WR-03, WR-02, WR-1.5 y WR-01) y un Planar Goubau Line (PGL). El diseño se ha realizado para cuatro diferentes rangos de frecuencias cubriendo desde 220 GHz hasta 1.1 THz. Utilizando como software de diseño CST.

El objetivo de este trabajo es evitar el uso de sondas y posicionadores, conectando así las guías de onda rectangulares directamente al VNA (Analizador Vectorial de Redes), aliviando los problemas de incertidumbre causados por dichas sondas.

Introducción

Las ondas milimétricas aparecieron en la década de 1890 cuando Lebedew, usando técnicas similares a las de Hertz, generó y detectó ondas cuya longitud estaba en torno a los 6 mm. Pero no fue hasta la Segunda Guerra Mundial, cuando la necesidad de obtener una mejor resolución angular en el radar de apertura, propició el uso de frecuencias más altas.

Durante muchos años las ondas submilimétricas sólo fueron aplicadas a campos como el de las ciencias espaciales o el de la espectroscopía molecular. Sin embargo, el nuevo milenio trajo la expansión de las aplicaciones de THz, sobre todo, aquellas relacionadas con el estudio de los efectos biológicos provocados por la radiación en ese rango de frecuencias. La radiación de THz se engloba dentro de la radiación no ionizante, es decir, no provoca daño a las estructuras moleculares, pero permite obtener información de las membranas celulares ya que la permeabilidad de éstas cambia con la frecuencia. Este cambio de permeabilidad es debido a la resonancia de sus biomoléculas.

En la Figura 1.1, se puede observar dónde se encuentra la región de THz dentro del espectro de frecuencias. Durante años, se refirió a este rango de frecuencias como la "región prohibida" (THz gap), ya que debido a su longitud de onda las aplicaciones de las regiones adyacentes, es decir, infrarrojos y microondas, no eran aplicables. Sin embargo, este problema se resolvió gracias a la aparición de fuentes de luz y detectores para THz.

Las investigaciones actuales se centran en el diseño de nuevos sensores y circuitos.

El uso de sondas y posicionadores, y la necesidad de cambiar varias veces la estructura hace que las medidas no sean tan exactas como debieran. Por eso, en este PFC se ha diseñado una transición, basada en guías de onda rectangulares, cuyo objetivo es evitar el uso de sondas, acabando así, con la incertidumbre en las medidas. Además de guías de ondas rectangulares, el sensor está compuesto por guías de onda coplanares (CPW) y por una Planar Goubau Line (PGL) (biosensor). En la Figura 2.1 se puede observar el sensor completo.

Teoría

En este apartado se puede leer un breve resumen teórico de las partes que componen el sensor.

Guía de onda rectangular

Una guía de onda rectangular es un componente lineal que transmite ondas electromagnéticas entre sus extremos, Figura 2.2. Ya que sólo hay un conductor, no se propagan modos TEM. El modo principal en una guía de onda rectangular es el modo TE_{10}, Figura 2.4.

Para comprobar si el diseño era escalable cuando se subía en frecuencia, se diseñaron cuatro transiciones. El tamaño de la guía de onda rectangular varía en cada rango de frecuencia, 0.86 × 0.43 [mm] (WR-03), 0.508 × 0.254 [mm] (WR-02), 0.381 × 0.1905 [mm] (WR-1.5) y 0.254 × 0.127 [mm] (WR-01). WR-03 va de 220 GHz a 325 GHz, WR-02 de 325 GHz a 500 GHz, WR-1.5 de 500 GHz a 750 GHz y WR-01 de 750 GHz a 1.1 THz.

La frecuencia que se usó como frecuencia de operación es la frecuencia intermedia para cada uno de los rangos. Es decir, 272.5 GHz para WR-03, 412.5 GHz para WR-02, 625 GHz para WR-1.5 y 925 GHz para WR-01.

Guía de onda coplanar

CPW es una línea de transmisión que tiene dos tierras separadas por un conductor central sobre un substrato, véase Figura 2.5.

Las ondas electromagnéticas no son solo transmitidas por el conductor, sino también por el substrato y el aire. Puesto que la onda viaja en un medio inhomogéneo el modo que soporta la CPW es Quasi-TEM, Figura 2.6. El porqué de usar CPW en vez de microstrip a pesar de su comportamiento similar, es porque a altas frecuencias CPW presenta menos pérdidas. Además a la hora de la fabricación, CPW es más fácil de construir.

Goubau Line

PGL es una línea formada por un conductor sobre un substrato, véase Figura 2.7.

El modo que se propaga en la PGL es el modo Quasi-TEM. El campo se extiende más allá de la línea, lo que la hace útil para espectroscopia celular, Figura 2.8. Algunos estudios, muestran que esta línea es muy sensible a cambios en la permitividad, lo que permite el análisis del biomaterial que se ubique sobre ella.

Diseño de la Transición

Puede decirse que en este PFC hay dos transiciones, que juntas, dan lugar al sensor que se utilizará para tomar información de las membranas celulares.

Primera transición: de guía rectangular a CPW

En las figuras 3.1 y 3.2 se pude observar la transición "desde dentro".

El campo entra por el Puerto 1 y llega al substrato, dónde tiene que acoplarse, para ello están la distancia $\lambda/4$, el cortocircuito (short) y la *probe*. La distancia $\lambda/4$ y el cortocircuito en la parte superior de la guía provocan un rebote del campo hacia atrás, la *probe* ayuda a dirigir el campo fuera de la guía de onda rectangular, a través de una apertura lateral. La *probe* es una placa metálica, usualmente con forma rectangular que se coloca en la superficie del substrato.

Una vez que el campo se acopla, y cambia de modo TE_{10} a modo CPW, sigue a través de un conductor que terminará siendo el conductor de la CPW.

Para diseñar esta transición hay que tener varios puntos en cuenta.

Para las cuatro guías de onda, los criterios de diseño, fueron los mismos. Por tanto de aquí en adelante, y hasta la sección de Resultados, la transición explicada será la que tiene a WR-03 como guía de onda rectangular.

La elección del substrato

En la guía de onda rectangular tiene que haber un substrato integrado. Para probar que substrato era el más adecuado, en CST, se modeló una guía rectangular con dos puertos y se insertó un substrato, véase Figura 4.2. Los substratos elegidos fueron Silicio (ϵ'_r = 11.9), Cristal (ϵ'_r =4.9) y Duroid (ϵ'_r =2.2). El grosor del substrato primero se estableció a 150 μm.

Los requisitos tomados para dar el resultado como válido, fueron que el parámetro S_{11} fuera menor que -10 dB y que el S_{21} fuera mayor que -1 dB.

En las Figuras 4.3, 4.4 y 4.5 puede observarse cómo, para cumplir con los requisitos, hubo que disminuir el grosor del substrato hasta 50 μm. Además, el único material que los cumple con ese grosor, es el Duroid.

Tamaños de las aperturas

Una vez elegido el material dieléctrico y el grosor que tendrá el substrato, se modelan las aperturas de la transición. Cuya finalidad es ayudar a que el campo se acople al substrato.
En las Figuras 4.11 y 4.12 pueden verse las aperturas horizontal y vertical.

Apertura Horizontal

Decidir el tamaño de la apertura horizontal es el primer paso de la optimización. Este tamaño está relacionado con la longitud de onda a la frecuencia de corte de la guía de onda rectangular. Por tanto, el tamaño elegido siempre será mayor que dicha longitud, véase Tabla 4.2.

Los resultados pueden observarse en la figura 4.13 a) y b). No hay gran diferencia entre ellos, pero para seguir con el segundo paso de la optimización, se tomó 0.84 mm como el resultado más óptimo.

Apertura Vertical

El tamaño de la apertura vertical está directamente relacionado con los modos de la CPW. En la Figura 4.15 se puede observar cómo si la apertura es demasiado pequeña el campo no pasa correctamente a través y si es demasiado grande no se acopla al substrato.

En los resultados, véase Figura 4.16 a) y b), se comprueba cómo el valor óptimo está entre medias del substrato y el cortocircuito (short), alrededor de 50 μm independientemente de la frecuencia.

Strip y tierras de la CPW

El siguiente paso de la optimización, hace referencia más directamente a la CPW.

En la Figura 4.18, pueden observarse más claramente ambos componentes.

El strip se utiliza para acoplar la *probe* a la CPW, el único requisito, en cuanto a la longitud, es que no puede ser muy corta porque entonces no deja al campo propagarse. En cuanto al grosor, de la Figura 4.21, se puede concluir que cuando la frecuencia aumenta el grosor disminuye.

En la Figura 4.19 se detallan las diferentes configuraciones para las tierras de la CPW. Si éstas son perpendiculares al campo, provocan reflexiones. La diferencia entre la forma diagonal y la redondeada es que con la redondeada el ancho de banda es mayor, como puede observarse en la Figura 4.20

Probe

La probe suele tener forma rectangular, sin embargo cuando se sube en frecuencia, los resultados mejoran si la forma cambia de rectangular a triangular, véase Figura 4.23.

Via Holes

Por último, el substrato no puede cortar a la guía totalmente, ya que el campo necesita sentir la continuidad de ésta.

Para la simulación se utilizaron paredes para conectar ambas secciones de la guía rectangular, sin embargo en la fabricación, esto no es posible debido a la dificultad de hacer esquinas. Por tanto, es necesario, cambiar esas paredes por unos pequeños cilindros metálicos (Via-Holes).

En la Tabla 4.3, se encuentran los distintos tamaños de los Via-Holes para las diferentes frecuencias. Para llegar a esos tamaños se siguieron las indicaciones dadas en [24], [25] y [26].

En la Figura 4.26 puede observarse la diferencia de resultados al usar paredes y al usar Via Holes.

Segunda transición: de CPW a PGL

La forma de esta segunda transición puede observarse en la Figura 4.18.

Las partes de la transición que forman parte de la optimización, son el grosor del substrato y la anchura de la PGL.

En el apartado de la elección del substrato, los resultados que pueden encontrarse en la Tabla 4.1 indican que cuánto más alta es la frecuencia más pequeño tiene que ser el grosor del substrato, ya que éste está relacionado con la longitud de onda del campo que tiene que pasar a través. Puesto que la primera y la segunda transición tienen que acoplarse perfectamente para evitar pérdidas, el grosor del substrato de ambas tiene que coincidir. En la Figura 4.29 se puede observar la actuación de cada uno de los grosores a una determinada frecuencia. Aunque todos los resultados son aceptables, se hace obvio mirando al parámetro S_{11} que cuanto más fino es el substrato más transparente le resulta al campo y menos se refleja.

En cuanto a la anchura de la PGL, ésta tiene que ser menor que el valor de la anchura del conductor de la CPW, es decir, 50 μm. En la Figura 4.30 se observa cómo para anchuras menores que 30 μm los resultados prácticamente no varían.

Resultados

Durante la optimización de ambas transiciones los requisitos para tomar un resultado como aceptable eran que el parámetro S_{11} fuera menor que -10 dB, y que el parámetro S_{21} fuera mayor que -1 dB. Esto fue para conseguir que los resultados finales, a pesar de la acumulación de errores, fueran aceptables.
Sin embargo, para considerar como aceptables los resultados finales, es decir, después de unir las dos transiciones, el parámetro S_{21} puede ser de hasta -3 dB, lo que implica perder la mitad de la potencia que se transmite.

De 220 GHz a 325 GHz

Para este rango de frecuencias, también se comprobó cual era la diferencia entre utilizar paredes metálicas y Via-Holes en los resultados del sensor completo. En la Figura 5.1, una pérdida de -2 dB cuando se usan Via-Holes se puede observar, lo que implica una disminución del ancho de banda.
El ancho de banda para el resultado tomado con paredes metálicas es de 65 GHz, mientra que el ancho de banda con Via-Holes es de 40 GHz.
En las siguientes secciones, sólo se analiza el mejor caso, es decir, utilizando paredes metálicas.

De 325 GHz a 500 GHz

Al aumentar la frecuencia, aparecen más modos de substrato y radiaciones que deterioran los resultados como puede observarse en la Figura 5.2.

El ancho de banda cuando S_{21} es mayor que -3 dB, se reduce 5 GHz hasta 60 GHz.

De 500 GHz a 750 GHz

En este rango de frecuencias, se puede observar el mismo efecto comentado anteriormente, véase Figura 5.3. El ancho de banda se reduce hasta 30 GHz.
Si relajamos el criterio, y aceptamos que los resultados puedan tener un S_{21} mayor que -5 dB, el ancho de banda estaría alrededor de 90 GHz.

De 750 GHz a 1100 GHz

Para estas frecuencias, el S_{21} es menor que -5 dB. Para analizar donde se porducen las perdidas, realizamos una técnica llamada "De-embeding" dónde analizamos los resultados paso por paso, como se puede observar en la Figura 5.5.
De esta técnica podemos concluir que tras añadir la segunda CPW los resultados se deterioran demasiado como para considerarlos aceptables. Por tanto, el sensor es escalable hasta alrededor de 700 GHz.

En la Tabla 5.1 se demuestra el hecho de que a más frecuencia, más potencia se pierde debido a la radiación y a los modos de substrato.

Por último, también se comprobó como afectaba a los resultados que el substrato tuviera pérdidas. Los resultados pueden observarse en las Figuras 5.6, 5.7 y 5.8. De esta prueba, se pudo obtener que para que los resultados empeorasen considerablemente y S_{21} fuera menor que -5 dB, la tangente de pérdidas tenía que estar entorno a 0.03.

Fabricación

Durante el desarrollo de este PFC, también se estudiaron los posibles problemas que se encontrarían durante la fabricación del sensor.

Substrato

El problema con el substrato es la debilidad debido a lo fino que es su grosor. Este hecho, hace que se necesite un soporte metálico debajo del substrato. Sin embargo, este soporte no puede ser completo ya que ni la CPW ni la PGL pueden tener metal bajo el substrato. El modelo se puede observar en la Figura 6.1.

Via-Holes

El problema con los Via-Holes es que su diametro es muy pequeño, y el substrato donde van a ser "taladrados" muy fino. Sin embargo, las nuevas técnicas de laser en micromachining eliminan este problema.

Tolerancias

Las variaciones en las Aperturas horizontal y rectangular, ya fueron analizadas previamente.

La distancia de la probe a las paredes metálicas o Via-Holes, tiene que ser menor que $\lambda/4$ para evitar resonancias.
Mirando en la Figura 4.11, se puede observar la apertura $\lambda/4$, que como fue comentado anteriormente se utiliza para que el campo rebote en el cortocircuito y vuelva para acoplarse al substrato. En la Tabla 6.1 se encuentran los valores con los que ese tamaño $\lambda/4$ puede variar.
Se puede concluir que cuando la frecuencia aumenta, el sistema se vuelve mucho más sensible a cualquier cambio.

Conclusión

En este PFC, para llegar al modelo que se presenta, primero se tuvieron en cuenta diferentes aproximaciones que posteriormente fueron rechazadas, véase Appendix I.

Como ya se dijo anteriormente, el objetivo de este proyecto fue desarrollar una plataforma basada en guías de onda rectangulares para evitar el uso de sondas que

provocan inexactitud en las medidas. Y escalarlo hasta 1.1 THz.

A lo largo de este resumen he contado los puntos más importantes en los que se ha basado mi PFC. Como se ha podido observar, el diseño trabaja aceptablemente y es escalable hasta 700 GHz. Por tanto, no sólo ayudará a tomar medidas más exactas de material biológico sino que también ayudará a la investigación en este campo, cada vez más importante.

Contents

List of Figures

List of Tables

1
Introduction

The history of millimeter and sub-millimeter waves, also known as -terahertz radiation, terahertz waves, T-rays, T-waves, T-light, T-lux or THz-, starts in the 1890's when Lebedew generated and detected wavelengths around 6 mm, using techniques similar to Hertz's. But it was not until the end of 1930's when new coherent radio sources appeared (klystron and the cavity magnetron). These sources were used in radars during the World War II. The war contributed to move to higher frequencies, due to the will of getting better angular resolution from aperture radar, after it, the new sources were used to develop the millimeter and sub-millimeter spectrum region [1].

However, by that time, this sub-millimeter radiation was only applied to space science, molecular line spectroscopy and plasma diagnosis. New millennium brought the expansion of THz applications, components and instruments regarding the biological effects associated with the THz region [2][4], which allow researchers to distinguish different proteins or obtain different information from the cellular membrane through the changes in its permeability [3], due to the vibrational and rotational resonances of their biomolecules. Besides these instruments, other growing applications in the THz frequency range are related to security, as contraband detection or imaging, as tumor recognition.

Looking at *Figure 1.1*, where the THz region is located can be seen, during years this frequency range was referred as the "forbidden region" (THz gap) [30], because, due to the wavelength, nor microwave applications nor infrared techniques were applicable in this band. However, that issue was overcome with the appearance of sources of THz light and detectors.

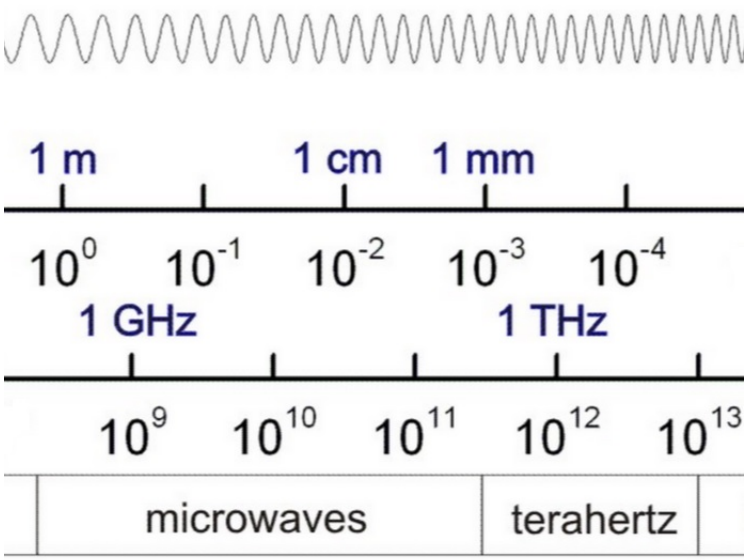

Figure 1.1: Electromagnetic spectrum in the millimeter and sub-millimeter wave region (THz band defined from 0.1 to 10 [THz])

Nowadays, the investigations in the radiation effect on biological samples, are focused on advances in circuit and device design, like the one carried out in this thesis, whose aim is to detect and control properties in the matter by using electromagnetic fields.
For THz measurements, using probs and positioners, the importance of placing them onto the calibration standards is crucial. Moreover, when measuring different biological material, it is need to obtain different measurements replacing the structure several times (repeatability), so getting good results and accurate measurements manually is completely challenging, even more when one of the goals is to move to higher frequencies.
The aim of this project is to design a transition from rectangular waveguide to Planar Goubau Line (sensing device) to be used with a biosensor in order to minimize the uncertainty consequence of probe misalignment. The misalignment gets worse when the frequency goes higher, because the device becomes more sensitive. That is, as it will be seen from the results in this thesis around 5 [μm] every [150 GHz], see *Table A.1.*
With the transition presented in this thesis, the porposed design overcome that problem, since the designed model is a structure always fixed. It is composed of two rectangular waveguides, a coplanar waveguide (CPW) and a planar goubau line (PGL), which is the bilogical sensing device.

During the next chapters the device will be explained, as well as some approximations that we also considered before getting the final model.

2

Theory

In the proposed transition, three different structures are used: rectangular waveguide, coplanar waveguide (CPW) and planar goubau line (PGL), see *Figure 2.1*.

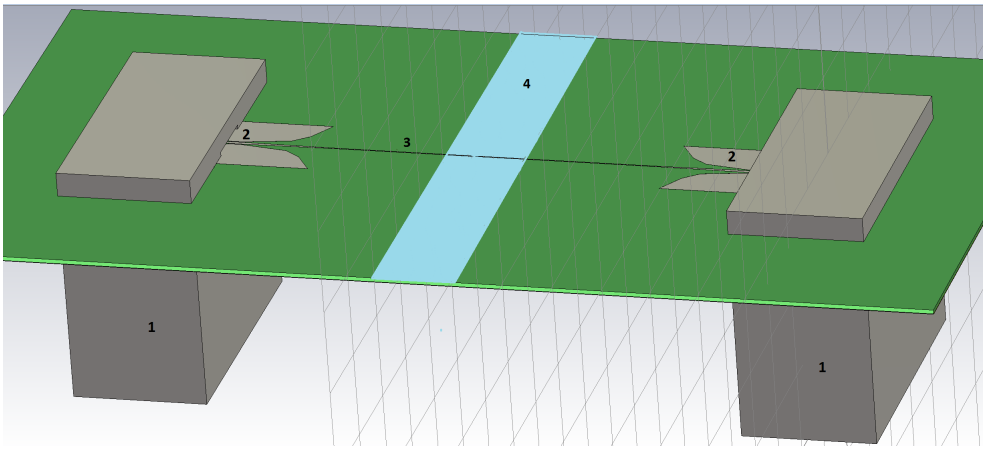

Figure 2.1: Proposed Transition. **1**. Rectangular Waveguide, **2**. Coplanar Waveguide, **3**. Planar Goubau Line. **4** Sensing Area

During this chapter these three structures will be theoretically described, as well as the S-Parameters, used for the transition design, the Vector Network Analyzer VNA, used for the experimental measurements, see *Section 2.4 and 2.5* respectively. And the software used to carry out the simulations, CST.

2.1 Rectangular Waveguide

Rectangular waveguide is a linear structure that transmits electromagnetic waves between its end points.

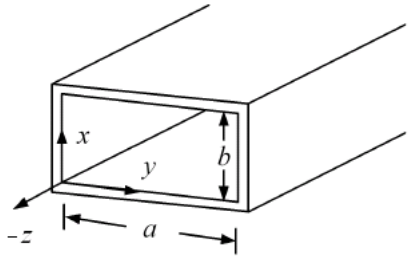

Figure 2.2: Rectangular Waveguide [33]

Remembering Maxwell equations [5][6], it is well known that each one of his equations solutions, in a transmission line, is called *mode*. If it is tranversal electric (TE), magnetic (TM), electro-magnetic (TEM) or Quasi-TEM depend on the value of the electric field and magnetic field longitudinal component.
The waveguide cavity can propagate TE and TM modes but not TEM since there is just one conductor. TE_{10} is the main mode for rectangular waveguides and TM_{11} for circular waveguides, since we are only using rectangular waveguides, in the following subsection just TE modes will be defined.

TE Modes

Since there is no longitudinal component of the electric field, in a rectangular waveguide the final solution for $\vec{H}$ is:

$$\vec{H}(x,y,z) = A_{mn}cos(\frac{m\pi x}{a})cos(\frac{n\pi y}{b})\epsilon^{-j\beta z} \tag{2.1}$$

where A_{mn} is the amplitude constant.
Following the method described in *Pozar* [5] or Collins [6], transverse field components of TE_{mn} mode are:

$$\vec{E_x} = \frac{j\omega\mu n\pi}{k_c^2 b}A_{mn}cos(\frac{m\pi x}{a})sin(\frac{n\pi y}{b})\epsilon^{-j\beta z} \tag{2.2}$$

$$\vec{E_y} = \frac{-j\omega\mu n\pi}{k_c^2 a}A_{mn}sin(\frac{m\pi x}{a})cos(\frac{n\pi y}{b})\epsilon^{-j\beta z} \tag{2.3}$$

$$\vec{H_x} = \frac{j\beta m\pi}{k_c^2 a}A_{mn}sin(\frac{m\pi x}{a})cos(\frac{n\pi y}{b})\epsilon^{-j\beta z} \tag{2.4}$$

$$\vec{H_y} = \frac{j\beta n\pi}{k_c^2 b}A_{mn}cos(\frac{m\pi x}{a})sin(\frac{n\pi y}{b})\epsilon^{-j\beta z} \tag{2.5}$$

Each mode has a cutoff frequency f_{cmn}

$$f_{cmn} = \frac{k_c}{2\pi\sqrt{\mu\epsilon}} = \frac{1}{2\pi\sqrt{\mu\epsilon}}\sqrt{(\frac{m\pi}{a})^2 + (\frac{n\pi}{b})^2} \tag{2.6}$$

The mode with the lowest f_{cmn} is the dominant mode. In case of the rectangular waveguide, since $a > b$, see *Figure 2.2*, the dominant mode is TE_{10}.

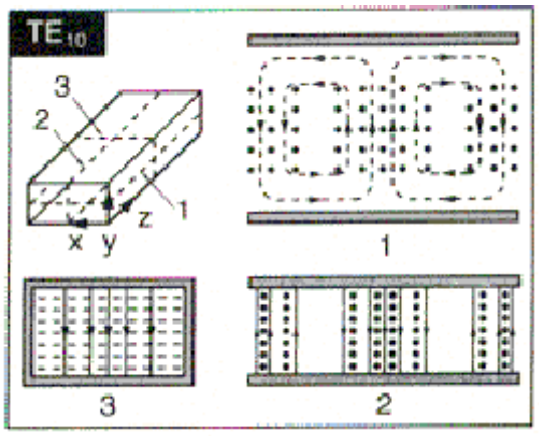

Figure 2.3: Mode TE_{10} in a rectangular waveguide [5]

In this thesis, four different rectangular waveguides are used, in order to test the scalability of our model when frequency increases. The four considered waveguides are: 0.86×0.43 [mm] (WR-03), 0.508×0.254 [mm] (WR-02), 0.381×0.1905 [mm] (WR-1.5) and 0.254×0.127 [mm] (WR-01). Their frequency ranges are:

$$WR - 03 = [220 - 325][GHz] \tag{2.7}$$

$$WR - 02 = [325 - 500][GHz] \tag{2.8}$$

$$WR - 1.5 = [500 - 750][GHz] \tag{2.9}$$

$$WR - 01 = [750 - 1100][GHz] \tag{2.10}$$

which means that from these frequencies main mode (TE_{10}) propagates, as in *Figure 2.4*.

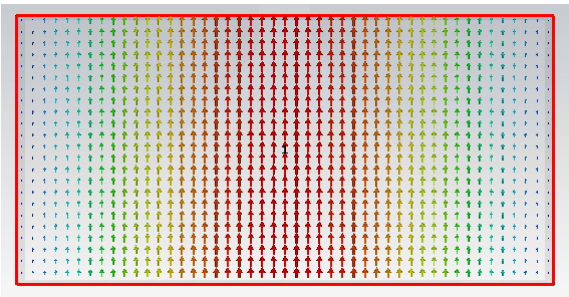

Figure 2.4: Mode TE_{10} for a rectangular waveguide simulated in CST, where the warmest colors refer to the highest power.

The used operating frequencies are the intermediate frequencies for each range, that is,

$$f_{WR3} = 272.5[GHz] \tag{2.11}$$

$$f_{WR2} = 412.5[GHz] \tag{2.12}$$

$$f_{WR1.5} = 625[GHz] \tag{2.13}$$

$$f_{WR1.5} = 925[GHz] \tag{2.14}$$

2.2 Coplanar Waveguide

CPW is a type of transmission line, which has a centered conductor separated from two ground planes on top of a dielectric substrate, see *Figure 2.5*.

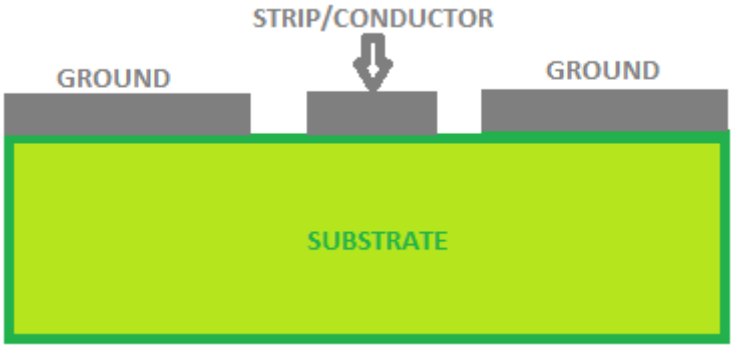

Figure 2.5: Coplanar Waveguide. The three lines on the top corresponds to the metallic conductor and grounds, below them, the dielectric substrate is located.

The electromagnetic wave is transmitted not only in the conductor but also in the substrate, and in the air. Since the wave is travelling in an inhomogeneous medium, the mode supported by CPW is not TEM but Quasi-TEM.

In this thesis we are working at high frequencies. For millimeter and sub-millimeter waves, CPW and microstrip work in a similar way. However, when impedance is high, as in the rectangular waveguide, CPW works better regarding to losses and dispersion, besides, it is easier to construct as no back processing is needed [7][8]. That is the reason why we used a CPW to match the rectangular waveguide and the PGL.

Once that waveguide mode reach CPW, rectangular waveguide mode becomes into the Quasi-TEM mode showed in *Figure 2.6*,

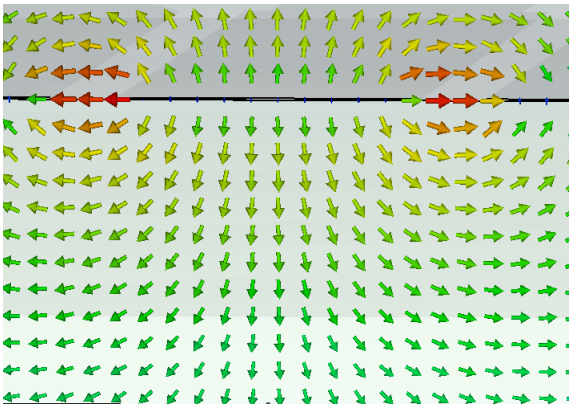

Figure 2.6: Quasi-TEM mode supported by a CPW simulated with CST. The warmest colors refer to the highest power.

2.3 Planar Goubau Line

PLG, is formed by a conductor strip over a substrate (*Fig*2.7).

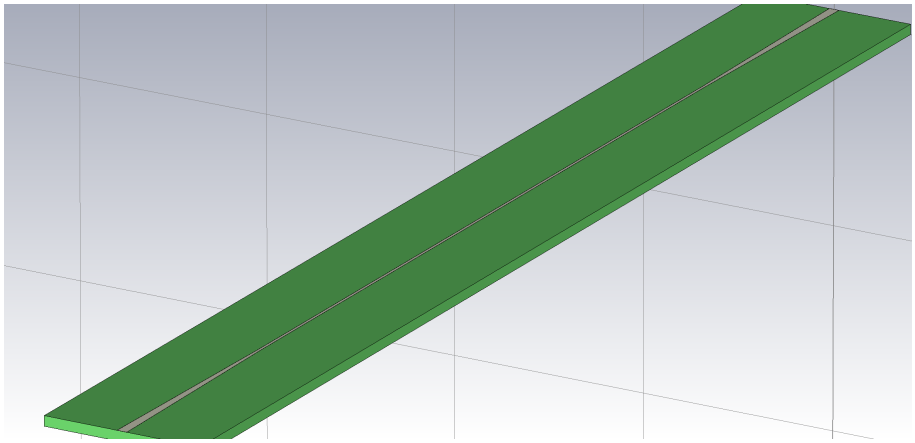

Figure 2.7: Planar Goubau Line

The propagating mode supported by the PLG is Quasi-TEM, the dielectric substrate around the wire reduces the radiated losses [9]. Using PGL for cell spectroscopy is useful since the field extends further from the line than in the CPW. Some studies, as the carried out by [9], show that the structure is sensitive to the permittivity change, even more if the wire size decreases. These features allow the analysis of different bio-material placed onto the line.

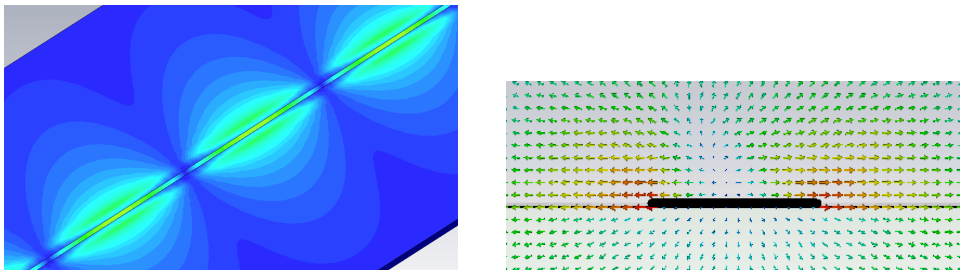

Figure 2.8: Top View and Cross Section of a Planar Goubau Line. The warmest colors correspond to the highest power.

2.4 S-Parameters

In order to characterize a device in a wave guiding system, the parameters used are the magnitude and phase of the transmitted and reflected waves [10]. The transmitted and reflected power is described by the scattering parameters. Equivalent voltages and currents, impedance and admittance matrices are impossible to measure directly but once scattering parameters are calculated, they can be obtained.
Transmitted and reflected waves have different amplitudes, they will be called, V_n^+ and V_n^- respectively, where n refers to the port number. So the [S] matrix defined thanks to these incident and reflected voltage waves is,

$$\begin{bmatrix} V_1^- \\ V_2^- \\ \vdots \\ V_N^- \end{bmatrix} = \begin{bmatrix} S_{11} & S_{12} & \dots & S_{1N} \\ S_{21} & \dots & \dots & \vdots \\ \vdots & \vdots & \vdots & \vdots \\ S_{N1} & \dots & \dots & S_{NN} \end{bmatrix} \cdot \begin{bmatrix} V_1^+ \\ V_2^+ \\ \vdots \\ V_N^+ \end{bmatrix}$$

where each S element is equal to,

$$S_{ij} = \frac{V_i^-}{V_j^+} \tag{2.15}$$

The reflection coefficient is defined as the ratio between the amplitude of the reflected and the incident wave in the same port. With this parameter we can compute *Return Loss*, *Instertion Loss* and SWR [5][6].
Both ports have an impedance Z_{0n}, where n refers to the port, so, in order to generalize scattering parameters, wave amplitudes can be defined as,

$$a_n = \frac{V_n^+}{\sqrt{Z_{0n}}} \tag{2.16}$$

$$b_n = \frac{V_n^-}{\sqrt{Z_{0n}}} \tag{2.17}$$

where a_n is the incident wave and b_n the reflected one,*Figure 2.9*, always referred to the n port.

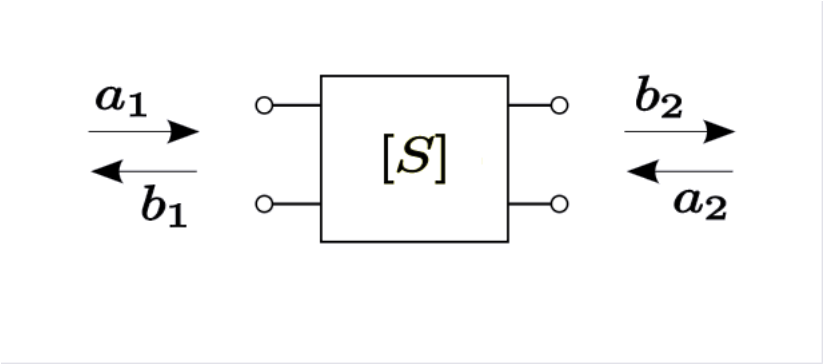

Figure 2.9: Two port network

Finally, expressions for voltage, current, and S parameters are:

$$V_n = V_n^+ + V_n^- = \sqrt{Z_{0n}}(a_n + b_n) \tag{2.18}$$

$$I_n = \frac{1}{Z_{0n}}(V_n^+ - V_n^-) = \frac{1}{\sqrt{Z_{0n}}}(a_n - b_n) \tag{2.19}$$

$$S_{ij} = \frac{b_i}{a_j} \tag{2.20}$$

2.5 Vector Network Analyzer (VNA)

Vector Network Analyzer is an equipment, *Figure 2.10* used for testing the performance of different devices with efficiency and precision, through the S-Parameters.

Figure 2.10: VNA equipment [32]

The main characteristic of a VNA is that it measures the magnitude and phase of the incoming and reflected waves, in order to generate the S-Parameters. Going back to the *Figure 2.9*, the magnitude is taken from the waves amplitude, and the phase from the mismatch between them. The incoming wave a goes from the VNA

to the DUT (Device Under Test) and the reflected, b, does it in the other way, *Figure 2.11.*

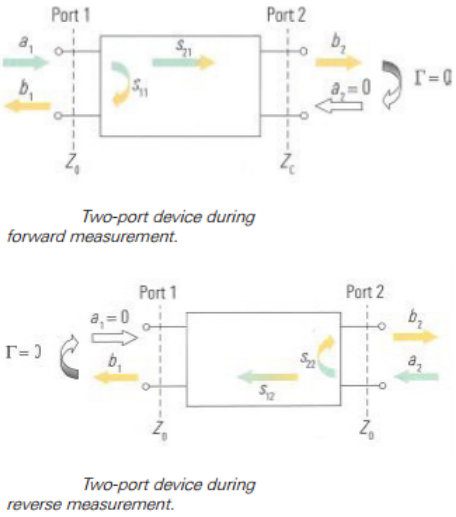

Figure 2.11: Measurements in a two-port device [32]

The main VNA advantage is the full error correction, which helps to compensate systematic errors, however for carrying out that correction *Calibration techniques* are needed (OSM, TRL, TRM, TOM, etc), more information regarding this techniques can be found in [32]. Moreover it can convert the data to time domain in order to improve the data interpretation. Embedding and Dembedding techniques are availabe, as well as the representation of the Smith Chart, see *Section 3.2.3 (Strip).*

2.6 Comptuer Simulation Technologsy Software (CST)

CST offers computational solutions for electromagnetic design and analysis [34]. Among the software that CST has, the one that is used in this thesis is CST Microwave Studio (CST MWS), which allow us to make a 3D EM simulation of the different parts that form our device, easing the analysis. Besides its fast and accurate analysis at high frequencies, CST also offers Time Domain solver and Frequency Domain solver.

3

Introduction to the transition

In this chapter I will do a brief explanation of how the the sensor works, for the reader to follow better the next chapter in which I will go through the different design steps.

In *Figure 3.1* it can be seen how the field, marked with a red arrow, is coming from the bottom of the rectangular waveguide. It goes through the substrate and reaches de top metal (short). The distance between the substrate and the short has to be $\lambda/4$, which makes the field reflects and go back to the substrate.

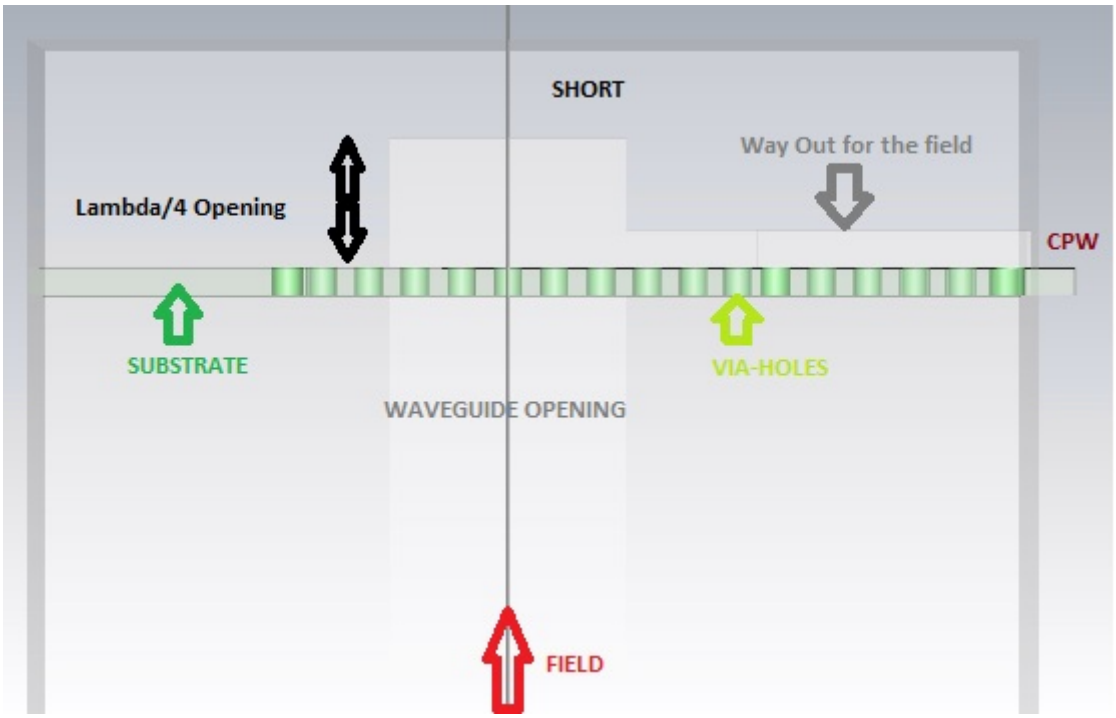

Figure 3.1: Side view of the rectangular waveguide

To help the field to couple into the substrate, there is a probe (small metal plate located over the substrate), see *Figure 3.2*. Moreover, the probe injects the field out of the rectangular waveguide through the strip that matches the rectangular waveguide to the CPW.

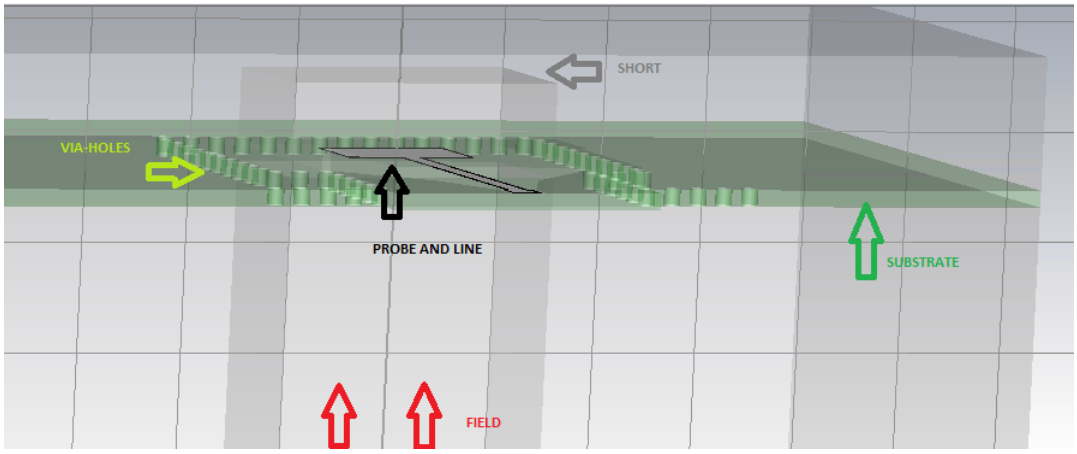

Figure 3.2: Front view of the rectangular waveguide

In *Figure 3.2* it can be also observed some cylinders, they are marked as Via-Holes. These Via-Holes make the rectangular waveguide to have a continuity, moreover they help to confine the field. In *Figure 3.1*, where the CPW is located can be seen, the CPW is the one which will feed the sensitive part of the device, the PGL.

Summarizing, in order to couple the field from the bottom part of the waveguide to the CPW, these considerations are needed:

- A short in the top side of the waveguide is needed. The distance from the dielectric to the short has to be $\frac{\lambda}{4}$ to provoke a reflection of the field.
- For the field to not to feel the discontinuity in the dielectric region, via holes connecting both sides of the waveguide are needed.
- An opening in one of the sides of the waveguide is needed to allow the field to propagate into the CPW.
- Once the field reflects at the short and goes back to the dielectric a probe and a line are needed to carry the field out of the waveguide through the side opening.

4

Device Design

In Chapter 2 the different parts that form our proposed device, i.e. Rectangular Waveguide, CPW and PGL, see *Figure* 2.1, were explained theoretically.
To make it easier to understand how we designed the device, it will be split in four different parts. In every part the design steps will be explained in detail.

4.1 Dielectric Material Election

As it was previously mentioned, our design is based on rectangular waveguides connected to the VNA, in order to avoid on-probe measurements. For the design of this sensor we will use an integrated substrate in the top part of the rectangular waveguide, see *Figure 4.1*, in order to couple the rectangular waveguide field into the substrate. Using that substrate and the metallic walls of the rectangular waveguide we will add the CPW [21], which will feed the PGL, key part for this project since the bio-material will be placed across that line *Figure 2.1, 4*.

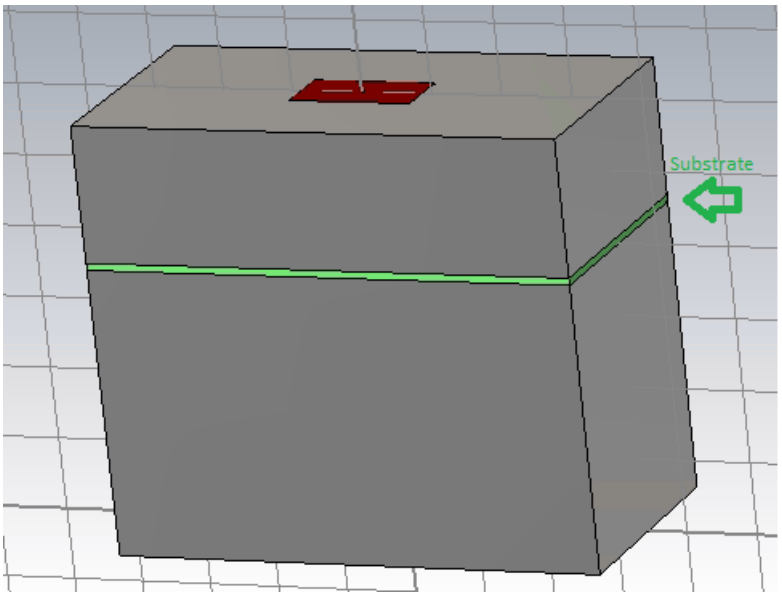

Figure 4.1: Rectangular waveguide with integrated substrate

The substrate of the CPW and PGL can be made of different dielectric materials, and these materials can have different thickness. Next, different materials and thicknesses will be studied.

In order to decide the appropriate material for the dielectric substrate, the modeled structure that we use is shown in *Figure 4.2*.

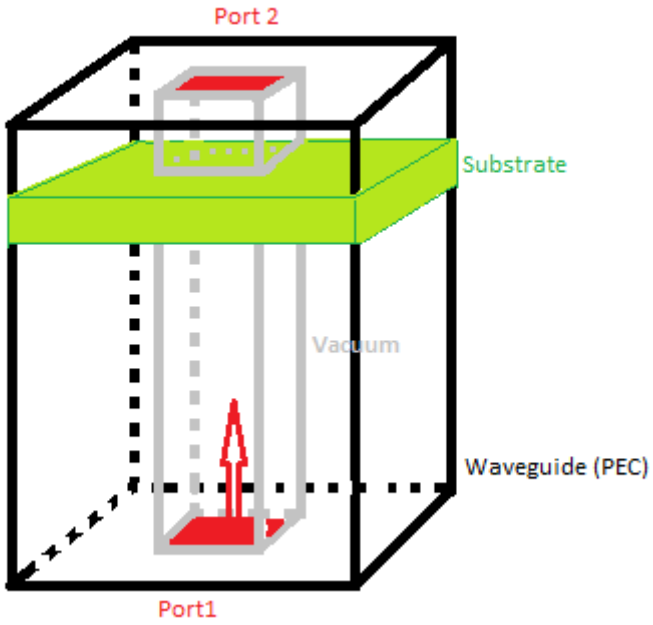

Figure 4.2: Simulation structure for testing dielectric materials. The incoming field from Port 1 reaches Port2 through the dielectric substrate.

As it can seen in the previous figure *Figure 4.2*, our waveguide has two ports and it is cut by a dielectric substrate. The incoming field from Port 1 is measured at Port 2 and the reflected power is measured at Port 1. The power that reaches Port 2 is measured by S_{21} and the reflected power is measured by S_{11}. From the S-Parameters results we decide if the material is adequate for our application and the thickness that it should have.
We take as a result good enough, the result for every material whose S_{11} is below -10 [dB] and its S_{21} close to 0 [dB], i.e. between 0 [dB] and -1 [dB].

The tested materials were Silicon ($\epsilon_r' = 11.9$), Glass ($\epsilon_r' = 4.8$) and Duroid ($\epsilon_r' = 2.2$). In the following subsections the different substrates will be analyzed for different frequencies.

WR-03

The frequency range of WR-03 goes from 220 [GHz] to 325 [GHz].

In the first test, a 150 [μm] dielectric substrate is used, results are shown in *Figure 3.5*.

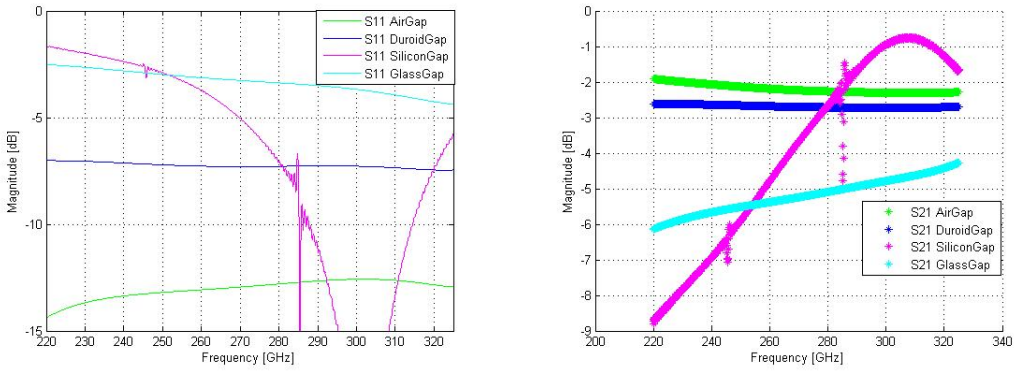

(a) $|S_{11}|$ (b) $|S_{21}|$

Figure 4.3: S-Parameters for different dielectric materials (Silicon, Glass and Duroid) with a substrate thickness of 150 [μm] compared to air. a) Magnitude of S_{11}. b) Magnitude of S_{21}

From, *Figure 4.3*, we can conclude that none of the dielectric materials work properly with a thickness of 150 [μm] at this range of frequency [200 - 325 GHz]. That is, S-Parameters do not follow the rule previously mentioned, in which, S_{11} has to be below -10 [dB] and S_{21} above -1 [dB]. We will reduce the substrate thickness until the S-Parameters results are adequate according to that rule. The next thickness tested is 100 [μm] and the results can be checked in *Figure 4.4*.

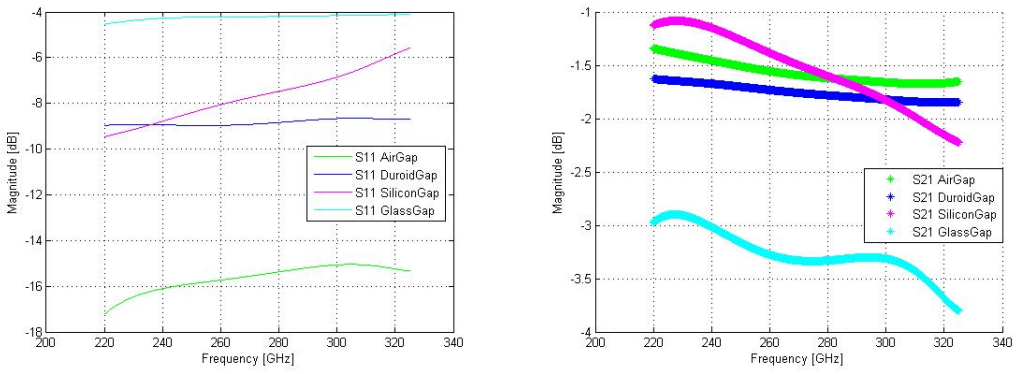

(a) $|S_{11}|$ (b) $|S_{21}|$

Figure 4.4: S-Parameters for different dielectric materials (Silicon, Glass and Duroid) with a substrate thickness of 100 [μm] compared to air. a) Magnitude of S_{11}. b) Magnitude of S_{21}

Still none of the S_{11} is below -10 [dB], so, for 50 [μm] thickness we obtain the results showed in *Figure 4.4*.

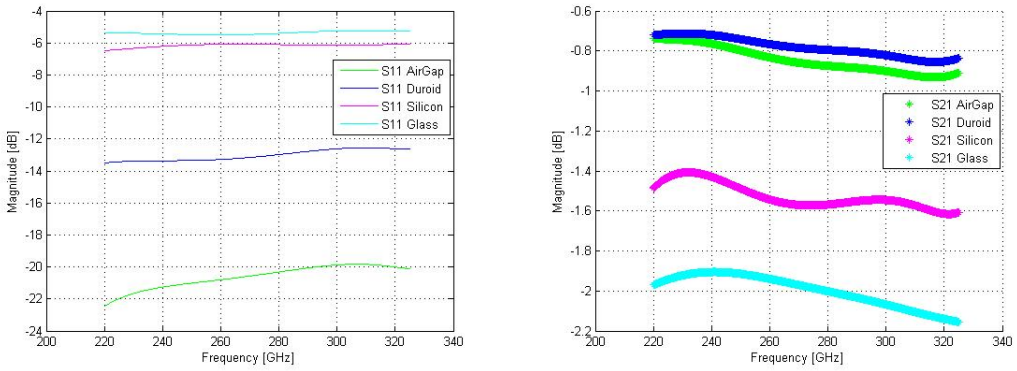

(a) $|S_{11}|$ (b) $|S_{21}|$

Figure 4.5: S-Parameters for different dielectric materials (Silicon, Glass and Duroid) with a substrate thickness of 50 [μm] compared to air. a) Magnitude of S_{11}. b) Magnitude of S_{21}

Now, it can be seen in *Figure* 4.4 how Duroid results are appropriate for this thickness, since S_{11} is below -10 [dB] and S_{21} is equal to -0.8 [dB]. If we continue decreasing the substrate thickness we would obtain better results, but the thinner is the material, the more difficult is the fabrication.

WR-02

WR-02 has a frequency range between 325 [GHz] and 500 [GHz].
In the previous subsection, it was demonstrated how the substrate thickness depends clearly on the frequency. The higher is the frequency the thinner must be the substrate has to be to reach the required standards. Considering the results for the WR-03 presented above, 50 [μm] will be the thicker substrate that we will consider for WR-02, see *Figure 4.6*. Moreover, Silicon or Glass will be also discarded as substrates due to their performance at lower frequencies.

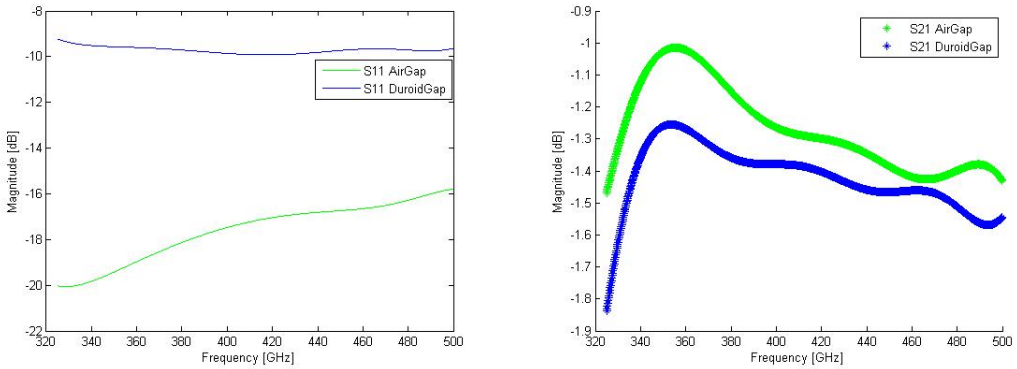

(a) $|S_{11}|$ (b) $|S_{21}|$

Figure 4.6: S-Parameters for Duroid compared with Air with a substrate thickness of 50 [μm] compared to air. a) Magnitude of S_{11}. b) Magnitude of S_{21}

In *Figure 4.6* it can be observed how S_{11} is still a little bit above -10 [dB], so we need to decrease the substrate thickness, in order to obtain a more adequate result. The next thickness tested was 30 [μm], its results can be checked in *Figure 4.7*.

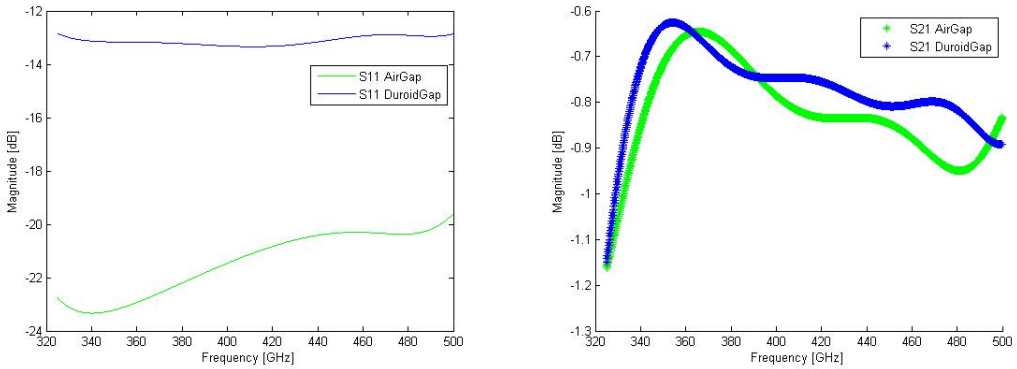

(a) $|S_{11}|$ (b) $|S_{21}|$

Figure 4.7: S-Parameters for Duroid compared with Air with a substrate thickness of 30 [μm] compared to air. a) Magnitude of S_{11}. b) Magnitude of S_{21}

As it was said previously, once S_{11} reaches -10 [dB] and S_{21} is close to 0 [dB] the result is taken as appropriate. In the case showed in *Figure 4.7*, for substrate of 30 [μm] thickness, S_{11} is below -10 [dB] and S_{21} is around -0.8 [dB].

WR-1.5

WR-1.5 frequency range goes from 500 [GHz] to 750 [GHz].
Following the previous steps, the thicker substrate tested at this frequency range will be 30 [μm]. For the S-Parameters simulated with a 30 [μm] substrate, the results obtained are showed in Figure 4.8.

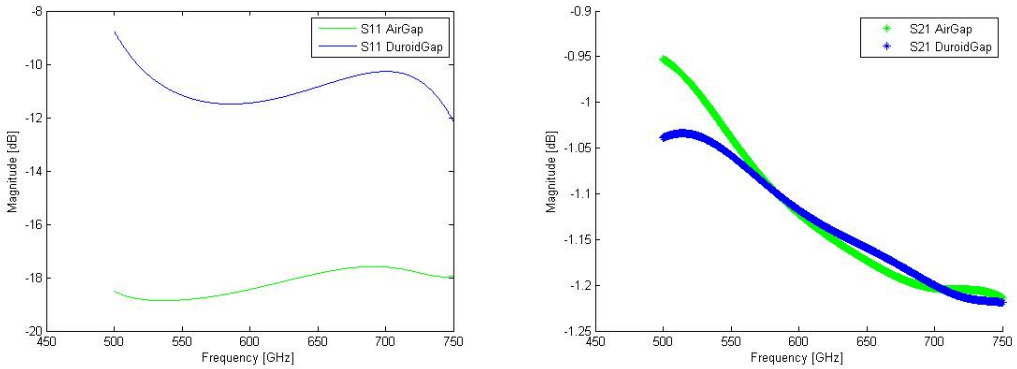

(a) $|S_{11}|$ (b) $|S_{21}|$

Figure 4.8: S-Parameters for Duroid compared with Air with a substrate thickness of 30 [μm] compared to the air. a) Magnitude of S_{11}. b) Magnitude of S_{21}

In *Figure* 3.12, we can see how S_{11} is clearly below -10 [dB] and S_{21} is around -1 [dB], approximately equal to -1.15 [dB], so 30 [μm] thickness is suitable for this frequency range.

WR-01

WR-01 is the waveguide which covers the frequency range from 750 [GHz] to 1.1 [THz].

Following the previous steps, the thicker substrate tested at this frequency range will be 30 [μm]. For the S-Parameters simulated with a 30 [μm] substrate, the results obtained are showed in *Figure 4.9*.

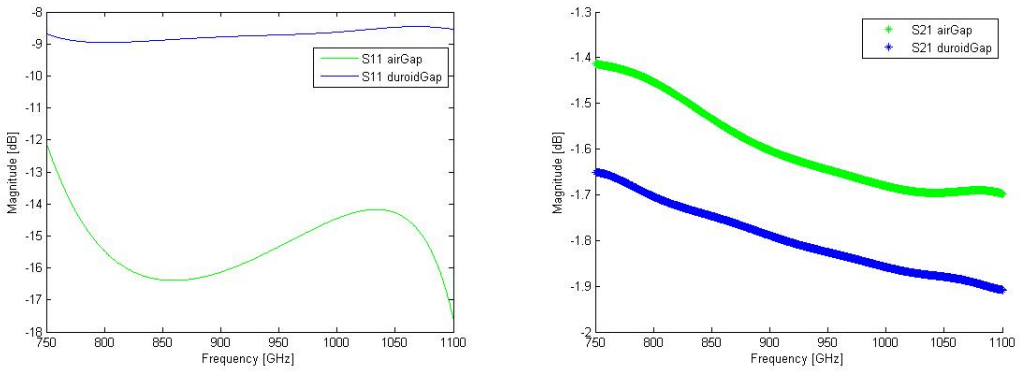

(a) $|S_{11}|$ (b) $|S_{21}|$

Figure 4.9: S-Parameters for Duroid compared with Air with a substrate thickness of 30 [μm] compared to the air. a) Magnitude of S_{11}. b) Magnitude of S_{21}

After analyzing the results obtained in *Figure 4.9*, we can conclude that Duroid do not work properly with a thickness of 30 [μm] at this range of frequency [750 - 1100 GHz]. That is, S-Parameters do not follow the rule previously mentioned, in which, S_{11} has to be below -10 [dB] and S_{21} around -1 [dB]. We will reduce the substrate thickness to 20 [μm]. The results for this thickness are shown in *Figure 4.10*.

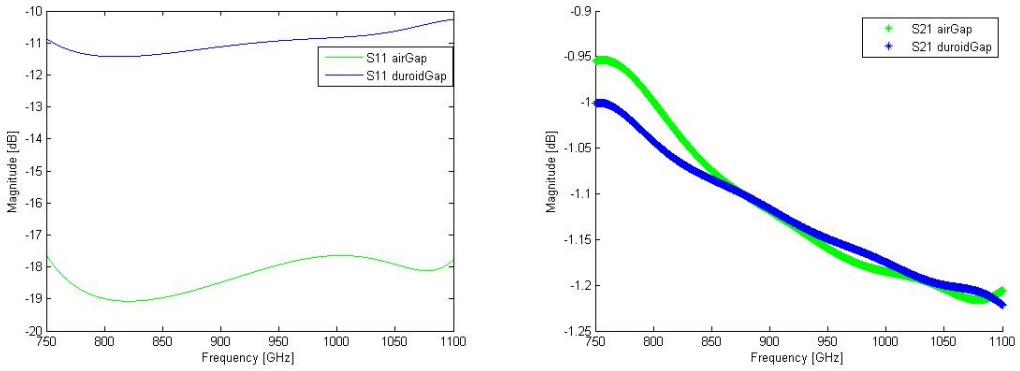

(a) $|S_{11}|$ (b) $|S_{21}|$

Figure 4.10: S-Parameters for Duroid compared with Air with a substrate thickness of 20 [μm] compared to the air. a) Magnitude of S_{11}. b) Magnitude of S_{21}

In *Figure* 4.10, we can see how S_{11} is below -10 [dB] and S_{21} is close to 0 [dB], around -1 [dB], that is why 20 [μm] thickness is suitable for that frequency range.

As conclusion, during the analysis, how materials with low permittivity performs better [22] has been observed, this is the reason why the selected material is the one with lower permittivity. In this case, Duroid is the chosen material, which has a relative permittivity of 2.2 [23]. In *Table 4.1* the frequency dependence of the Duroid and optimum substrate thickness is observed.

	WAVEGUIDE			
	WR3	WR2	WR1.5	WR1
Material	Duroid (ε = 2.2)			
Thickness	50 µm	30 µm	30 µm	20 µm

Table 4.1: Chosen material and thickness for the different waveguides

4.2 Rectangular Waveguide - Coplanar Waveguide Transition

In this section, the coupling between the rectangular waveguide and the CPW will be explained.

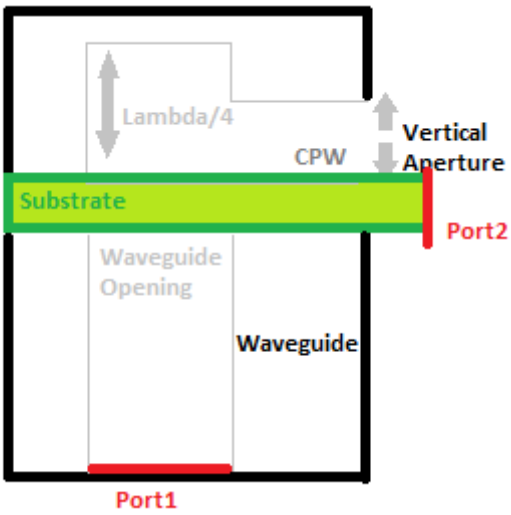

Figure 4.11: Side View of the rectangular waveguide and CPW transition

As the problem is too big to try to fix everything at the same time, we divided it in steps. Along this chapter, these steps will be follow in the same order for each one of the considered frequency ranges. The location of the ports, as well as the rest of the important points are marked in *Figures 3.1, 3.2, 4.11, 4.12*.

The design steps are:

- Horizontal Aperture
- Vertical Aperture
- Microstrip and CPW grounds
- Probe
- Walls vs. Via-Holes

4.2.1 Horizontal Aperture

In order to understand which part of the transition is referred as *Horizontal Aperture*, we can have a look to *Figure 4.12*.

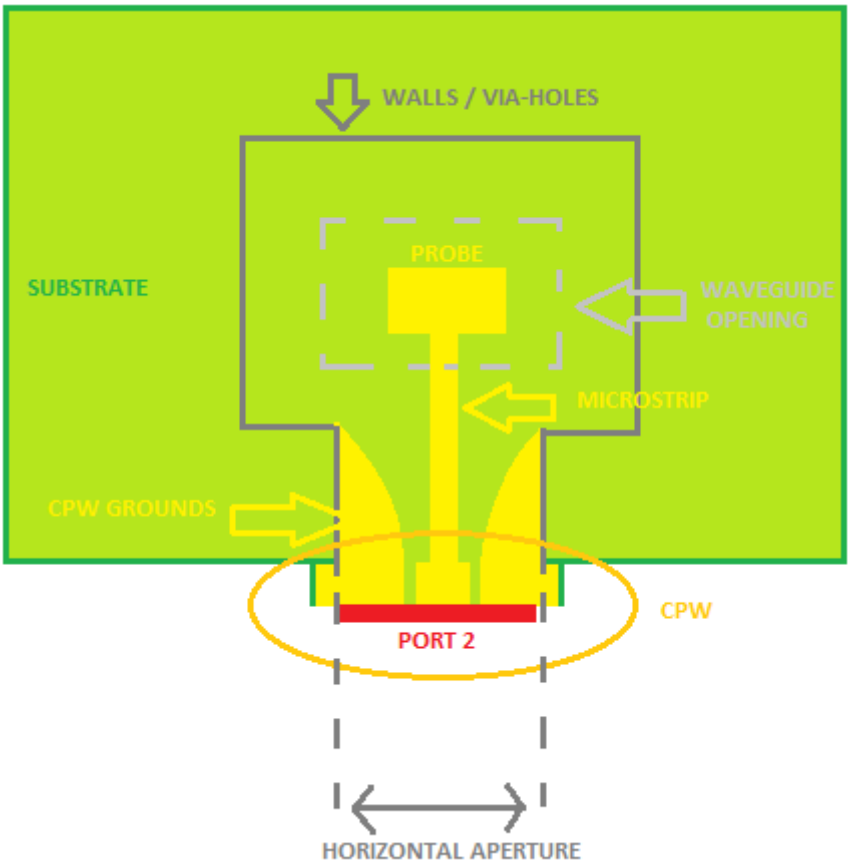

Figure 4.12: Top View of the rectangular waveguide to CPW transition

The size of the Horizontal Aperture is directly related to the cut off frequency for the rectangular waveguide mode TE_{10}. That is, the Horizontal Aperture has to be equal or bigger than the length of the guided lambda at the cut off frequency, otherwise the field would remain confined in the rectangular waveguide. Values of the guided lambda at the different frequencies studied are shown in next table, *Table 4.2*.

Frequency range [GHz]	λ_guided [mm]
220 – 325	0.81
325 – 500	0.49
500 – 750	0.36
750 – 1100	0.24

Table 4.2: Values of guided lambda and rectangular waveguide opening

Looking at the previous table, it can be seen how the size of the Horizontal Aperture can not be much smaller than the longest side of the waveguide opening, (a, see *Figure 2.1*).

To check the possible sizes of the Horizontal Aperture we will use the S-Parameters.

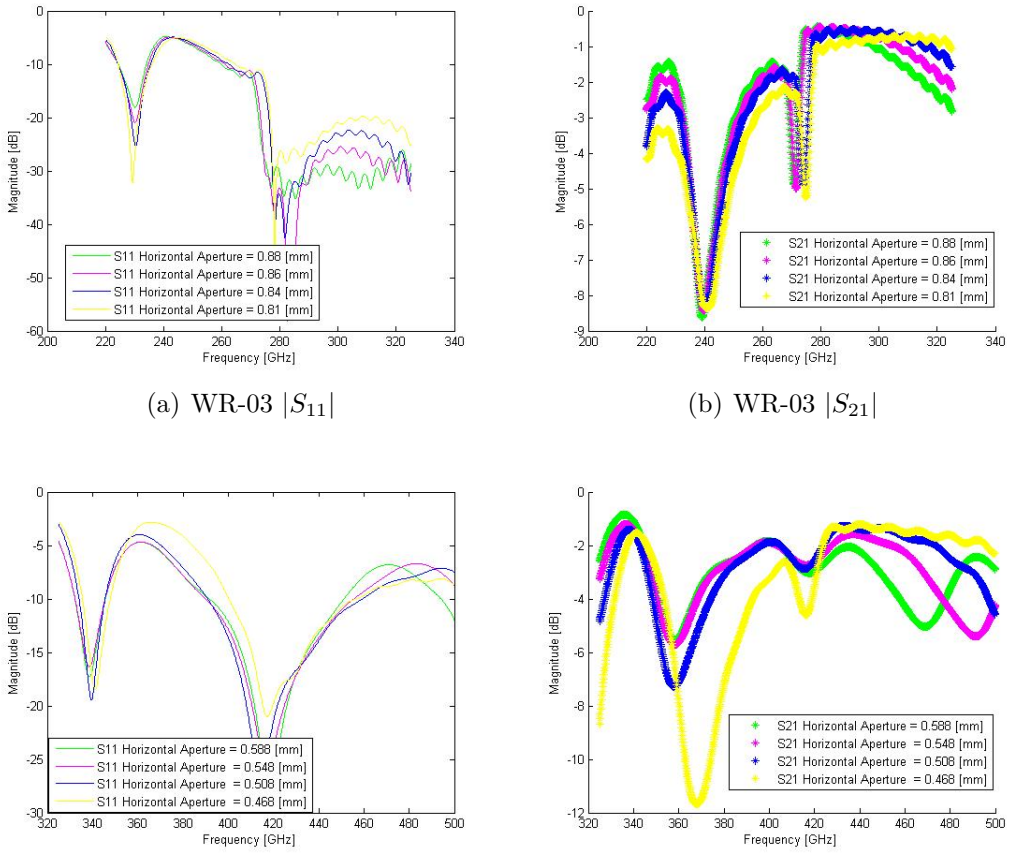

(a) WR-03 $|S_{11}|$

(b) WR-03 $|S_{21}|$

(c) WR-02 $|S_{11}|$

(d) WR-02 $|S_{21}|$

Figure 4.13: S-Parameters for the transition between WR-03/WR-02 and CPW for different values of the Horizontal Aperture.

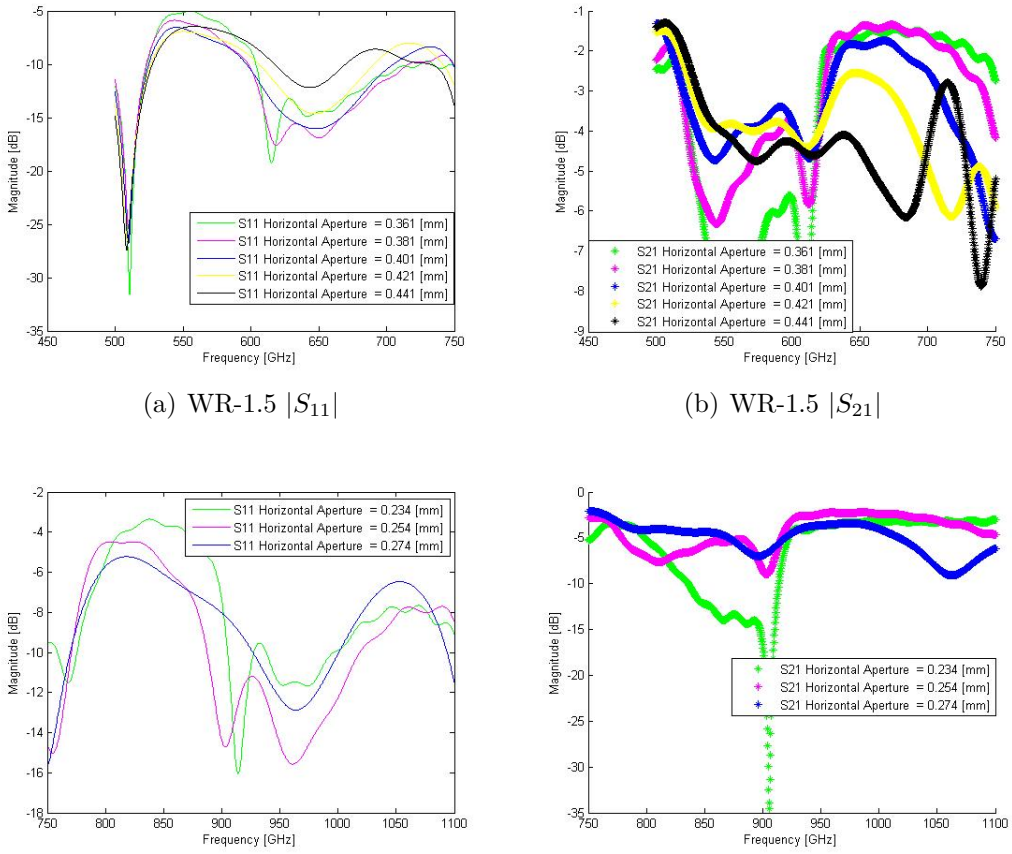

(a) WR-1.5 $|S_{11}|$

(b) WR-1.5 $|S_{21}|$

(c) WR-01 $|S_{11}|$

(d) WR-01 $|S_{21}|$

Figure 4.14: S-Parameters for the transition between WR-03/WR-02 and CPW for different values of the Horizontal Aperture.

This one, is the first optimization step, that is why the S-Parameters are not as appropriate as expected. Moreover, there is not a huge difference bettween the results, but still we took one of the sizes as the optimum value, in order to continue with the optimization. For the first waveguide, WR-03, aperture is going to be $0.84[mm]$, .The best result for the Horizonal Aperture in WR-02 is a. For WR1.5 the optimum result is obtained when the aperture is $0.401[mm]$ and in WR1 when is equal to $0.26[mm]$.

4.2.2 Vertical Aperture

In *Figure 4.11* Vertical Aperture can be seen. Once that we optimized the Horizontal Aperture for each frequency range, we modify the Vertical Aperture to continue improving the transition.

The size of the vertical aperture is directly related to the CPW modes. *Figure 4.15* shows how the CPW mode looks for different apertures.

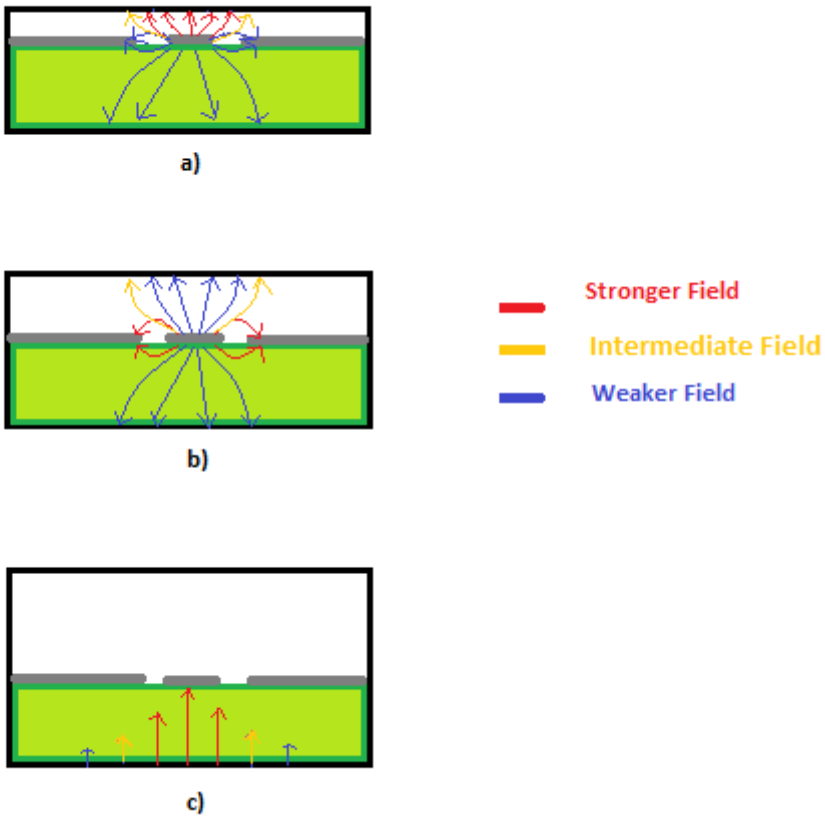

Figure 4.15: Field propagating in the CPW before getting out from the rectangular waveguide. a) When the ceiling is too close to the CPW b) Optimum case c) Extreme case, when the ceiling is too high and the field continue propagating as a TE mode

In *Figure 4.15* the three CPWs observed are still surrounded by the metal of the waveguide (black rectangle). When the ceiling is too close to the CPW the field does not propagate properly because it couples to the ceiling instead of coupling to the CPW, see *Figure 4.15, a)* . On the contraty, if the ceiling is too high the field does not couple to the CPW, and the TE_{10} does not adapt properly into the Quasi-TEM mode of the CPW, see *Figure 4.15, c)*. To get the optimum value for the vertical opening, S-Parameters will be used.

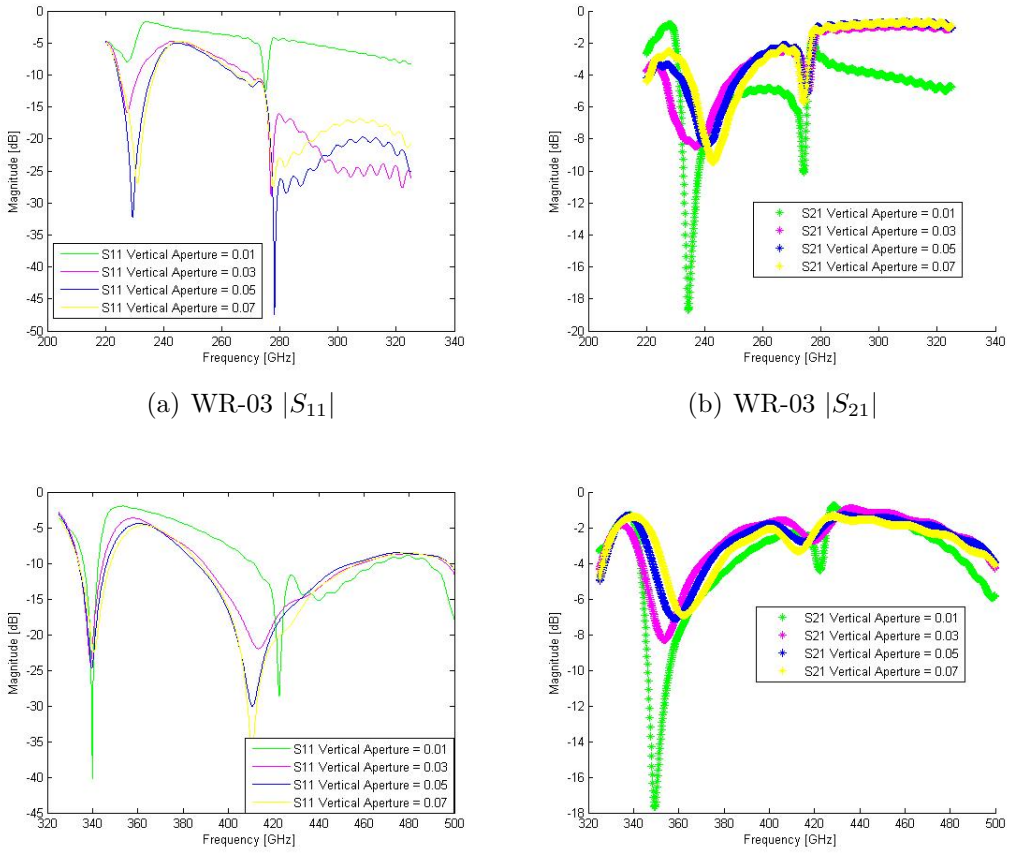

(a) WR-03 $|S_{11}|$

(b) WR-03 $|S_{21}|$

(c) WR-02 $|S_{11}|$

(d) WR-02 $|S_{21}|$

Figure 4.16: S-Parameters for the transition between WR-03/WR-02 and CPW for different values of the Vertical Aperture.

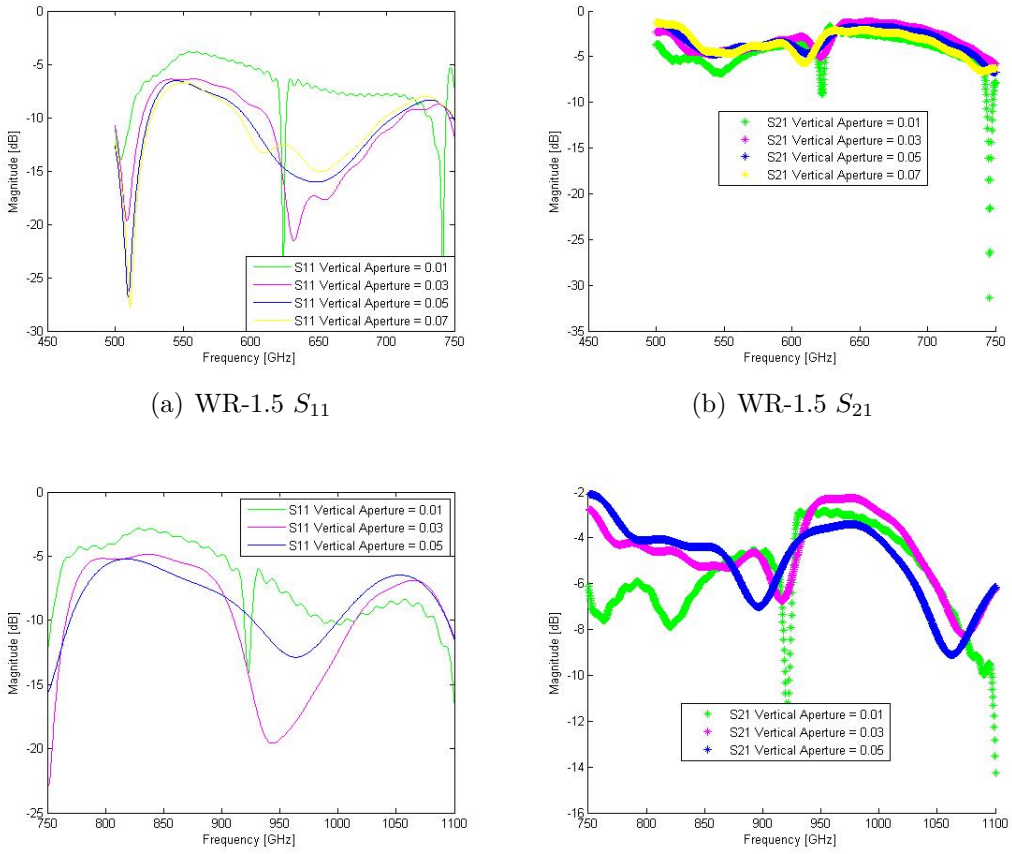

(a) WR-1.5 S_{11}

(b) WR-1.5 S_{21}

(c) WR-01 S_{11}

(d) WR-01 S_{21}

Figure 4.17: S-Parameters for the transition between WR-1.5/WR-01 and CPW for different values of the Vertical Aperture.

Analyzing the previous figures, we can see how, for all of the frequencies, if the aperture is not high enough (0.01 [mm]) the S_{11} is above -10 [dB] and S_{21} around -5 [dB], that is why we can conclude that for this size of the vertical aperture there is not a good coupling between the rectangular waveguide and the CPW. This improper response is due to the impossibility of field of going through the CPW until the Port 2. Also we can observe a similar behaviour when the aperture is too high (around 0.07 [mm]), since the modes are not changing properly.
We will take as the best result, the one which has a S_{21} between 0 and -3 [dB], and with the S_{11} that provides us with the wider bandwidth below -10 [dB].

The conclusion is that the optimum value for the Vertical Aperture is always around 50 [μm], independently of the frequency range. That is, looking at the previous figures, it is obvious that for 0.05 [mm], the S-Parameters performance is better.

4.2.3 Strip and CPW Grounds

None of the steps is more important than other, but if we focus on the matching between rectangular waveguide and CPW, this subsection and next one, take part

more directly in that issue. Previous sections were more into allowing the field to propagate. In *Figure 4.18* the important area for this subsection is shown.

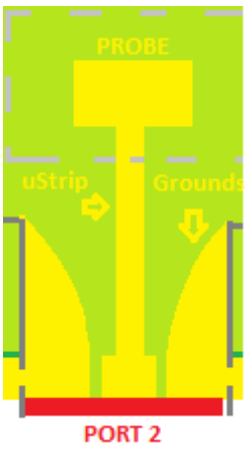

Figure 4.18: Microstrip and CPW grounds

CPW grounds

We will start with the the CPW grounds. As it was theoretically defined in Chapter 2, it is well known that the CPW has no ground in the bottom, but it has two grounds, one at each side of the conductor. In *Figure 4.19* we show different configurations for the starting of these grounds.

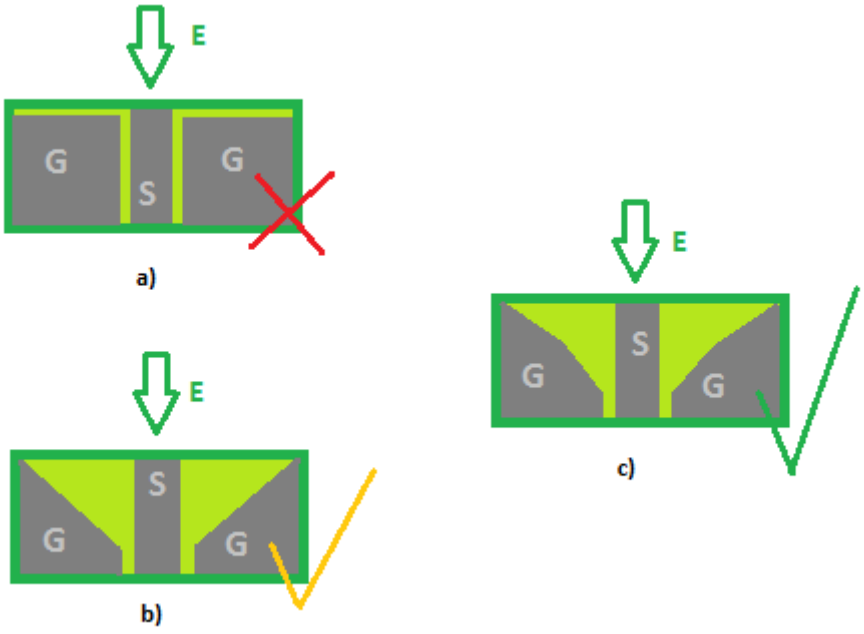

Figure 4.19: Different design of CPW grounds. a) Perpendicular Grounds, b) Diagonal grounds c) Round grounds. G: Grounds, S: Strip

If the electromagnetic field is coming in the green arrow direction, see *Figure 4.19*, and it finds suddenly perpendicular grounds *Figure 4.19 a)*, the field reflects more

than if the grounds are diagonal or round. The optimum result, as it can be seen in the next figure, *Figure 4.20* is better when they are round, because the field finds the change smoother, which provide us with a wider bandwidth.

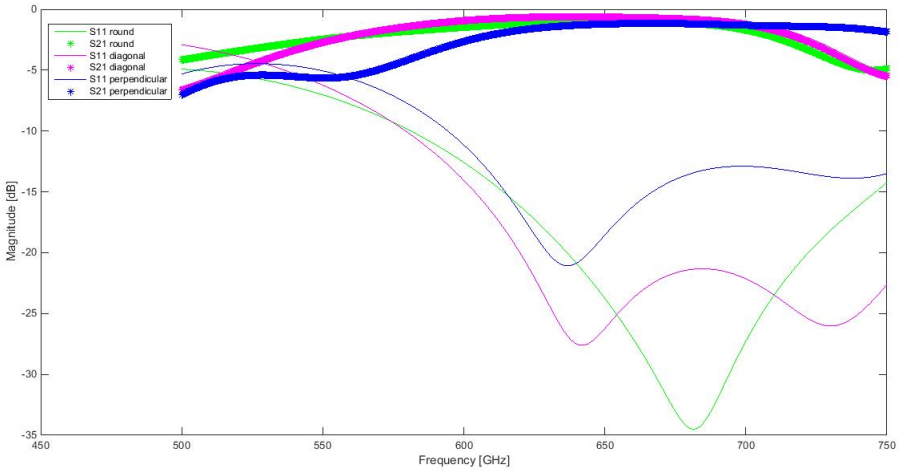

Figure 4.20: S-Parameters of the three ground possibilities with WR-1.5

Strip

Regarding to the strip, shown in *Figure 4.18*, there are two different things that can be modified, the length and the width.

The length cannot be too short, because in that way the field does not propagate. For everyone of the frequency ranges, the length is around the value of λ. Once the length of the strip is set, next step changes the strip width value between 0.01 [mm] and 0.05 [mm]. The width of the strip is also related to the wavelength, so, as we have different ranges of frequency, this study has to be split in four parts.

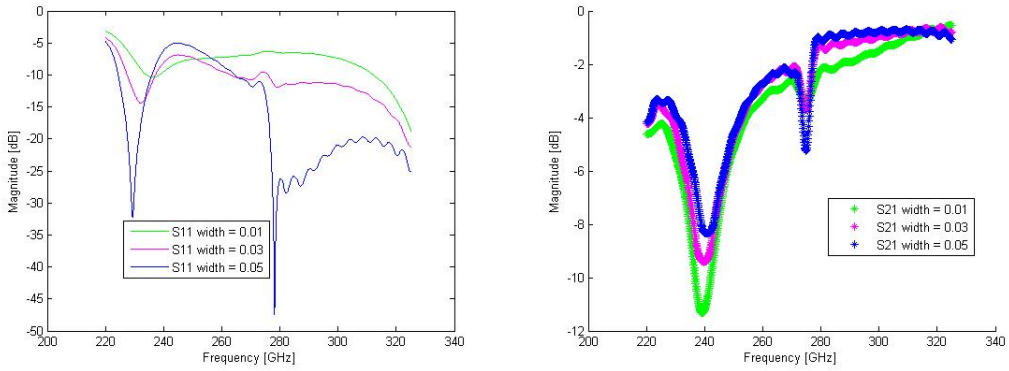

(a) WR-03 $|S_{11}|$ (b) WR-03 $|S_{21}|$

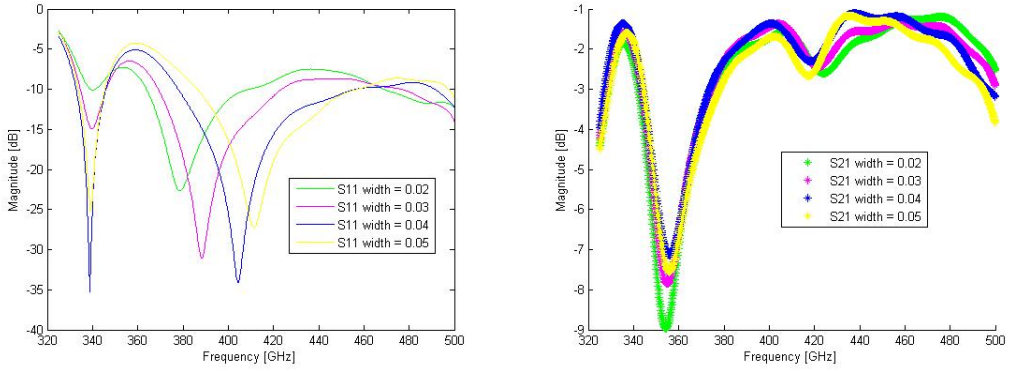

(c) WR-02 $|S_{11}|$ (d) WR-02 $|S_{21}|$

Figure 4.21: S-Parameters for the transition between WR-03/WR-02 and CPW for different values of the strip width.

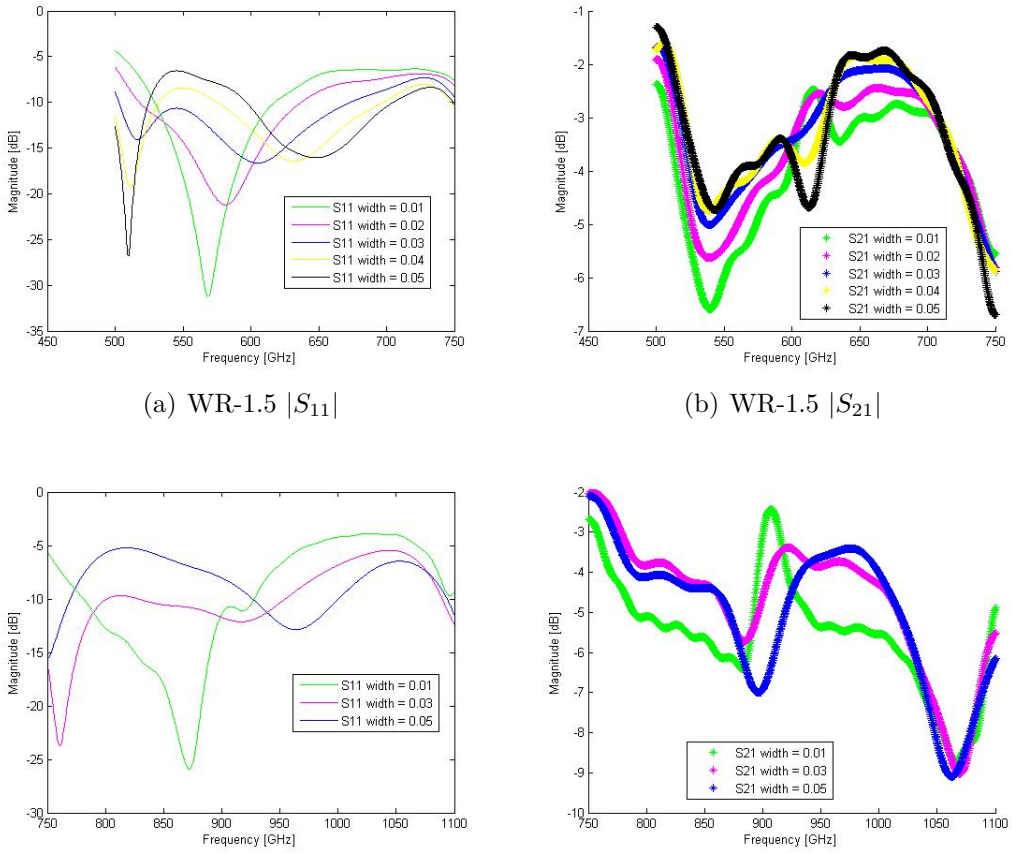

(a) WR-1.5 $|S_{11}|$

(b) WR-1.5 $|S_{21}|$

(c) WR-01 $|S_{11}|$

(d) WR-01 $|S_{21}|$

Figure 4.22: S-Parameters for the transition between WR-1.5/WR-01 and CPW for different values of the strip width.

Based on the results showed in *Figure 4.21 and 4.22*, we can conclude than when the frequency increases the strip width decreases.

4.2.4 Probe

Probes, see *Figure 3.21*, are pieces of metal, which can have different shapes, used mainly to capture the field and carry it through, in our case, the microstrip line. To inject the field out of the waveguide, the probe is located strategically in the middle of the waveguide opening over the substrate. If we have a look at *Figure 3.20*, we can see the probe location.

During this step we will have a look to different probe shapes, and how they affect the performance of the transition.

At the beginning, the four transitions were designed using a rectangular probe, since it is the most common one, but not for all of them the S-Parameters results were adequate. In *Figure 3.26* the S-Parameters results of the transition between WR-01 and CPW with rectangular probe are shown. In that figure, the results obtained with triangular probe can been also observed.

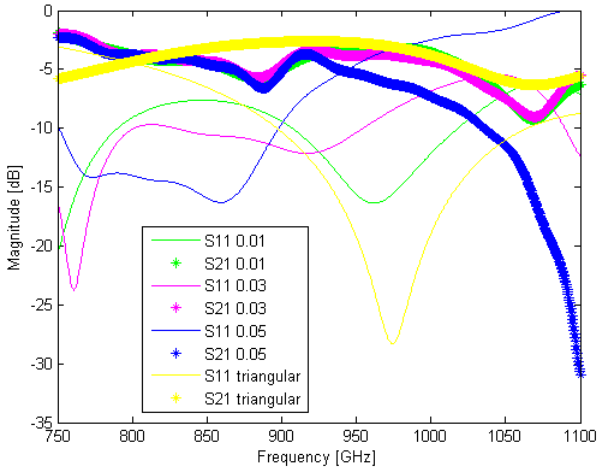

Figure 4.23: WR-01 to CPW transition using different widths [mm] of rectangular probe (green, pink and blue) and using triangular probe (yellow)

Analyzing *Figure 4.23*, the S-Parameters for the triangular probe are more stable than the S-Parameters for the rectangular probe, that is why we will use the triangular shape for frequencies above 500 GHz.
The results for the transitions that work with frequencies below 500 [GHz], are always better with rectangular probe, that fact can be checked in *Figure 3.24*.

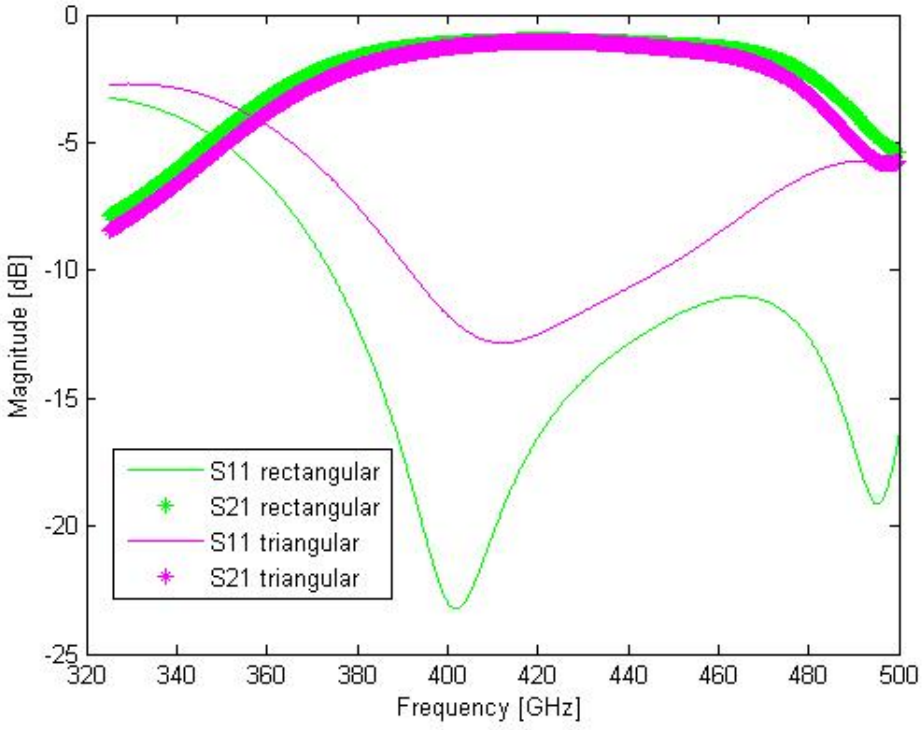

Figure 4.24: WR-02 to CPW transition using rectangular and triangular probes

To conclude this section, it is important to take into account that the probe cannot

cover completely the rectangular waveguide opening, no matter if it is rectangular or triangular, because then, the field would not go through the aperture and everything would be reflected back to the Port 1.

4.2.5 Walls vs. Via-Holes

Via-holes are metallic cylinders that connect both sides of the waveguide, and they are accurately made by drilling. For the fabrication perspective, the walls have to be changed by via-holes, see *Figure 4.12* to see where they are placed.

Once that all the parameters in the transition are optimized, we change the walls by the via-holes. Using either walls or via-holes similar results are obtained. To get these similar results, avoiding leakage between the vias, the calculations explained in [24][25] are used. Moreover, since these vias are oriented to the fabrication perspective, [26] recommends that their diameter has to be equal to the thickness of the substrate.

Following all the recommendations, our via-holes, see Figure 4.25, have the sizes showed in *Table 4.3*.

Figure 4.25: Via-Holes sizes

	WR3	WR2	WR1.5	WR1
Substrate Thickness [µm]	50	30	30	20
Via – Hole diameter [µm]	50	30	30	20
Separation between Via - Holes [µm]	75	50	50	30

Table 4.3: Via-Holes sizes

Since the transitions which use WR-02 and WR-1.5 have the same substrate thickness but a huge variation in frequency, they will be used to show the comparison between the performance with via-holes and with walls, see *Figure 4.26 and 4.27*.

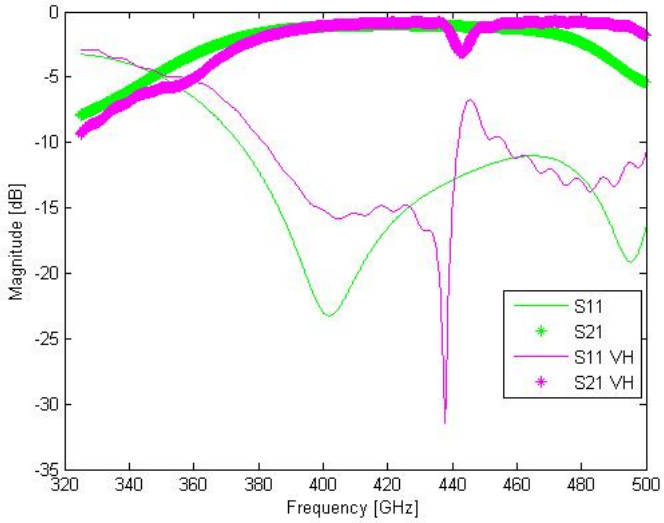

Figure 4.26: Walls vs. Via-Holes in WR-02 to CPW transition

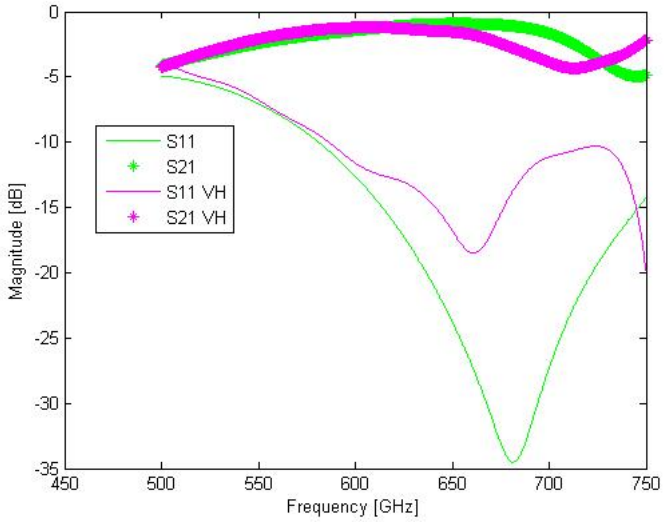

Figure 4.27: Walls vs. Via-Holes in WR-1.5 to CPW transition

In both figures, *Figure 4.26 and 4.27*, it can be seen how the Via-Hole performance follows quite accurately the one with walls independently of the frequency rising. In these figures a small resonance can be observed in the parameter S_{21} which is due to the distance between the probe and the walls/via-holes. This will be fixed and shown in the complete results in *Chapter 5*.

4.3 Transition between CPW and PGL

Until now we have described the transition between rectangular waveguide and CPW. Now we present the study of the transition between the CPW and the PGL, which is based on [27].

The transition between the CPW and PGL can be seen in *Figure 4.28*.

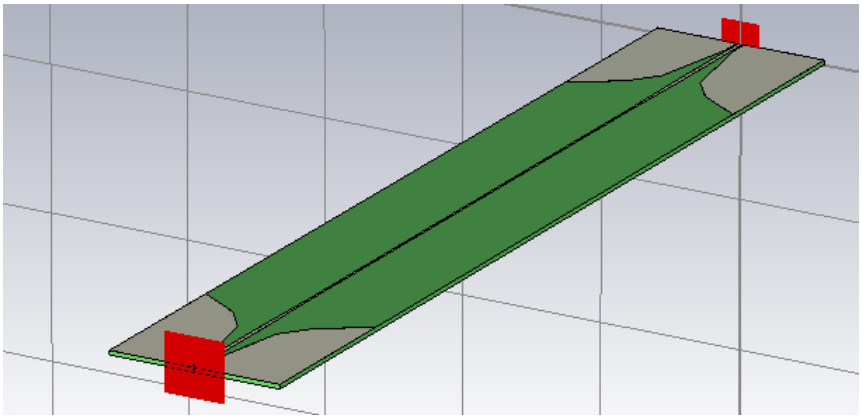

Figure 4.28: CPW to PGL transition based on the transition proposed in [27]

As it can be seen in *Figure 4.29* the grounds for the CPW are finished in the same way that they were started, see *Figure 4.19*, to make the field change smoothly from the CPW to the PGL.
To contribute to that smooth change, the CPW strip decreases also slowly until it reaches the width of the PGL, from 0.05 [mm] to 0.014 [mm].
What we need to test in this transition is how the substrate thickness and the width of the PGL affect the performance. The substrate thickness of the transition between the CPW and the PGL has to be the same that the thickness used for the transition between the rectangular waveguide and the CPW, in order to avoid reflections. That is why, we will see the performance of 50 [μm] thickness at [220 - 325 GHz], 30 [μm] thickness at [325 - 500 GHz] and [500 - 750 GHz] and 20 [μm] thickness at [750 - 1100 GHz]. Results are shown in *Figure 3.33*.

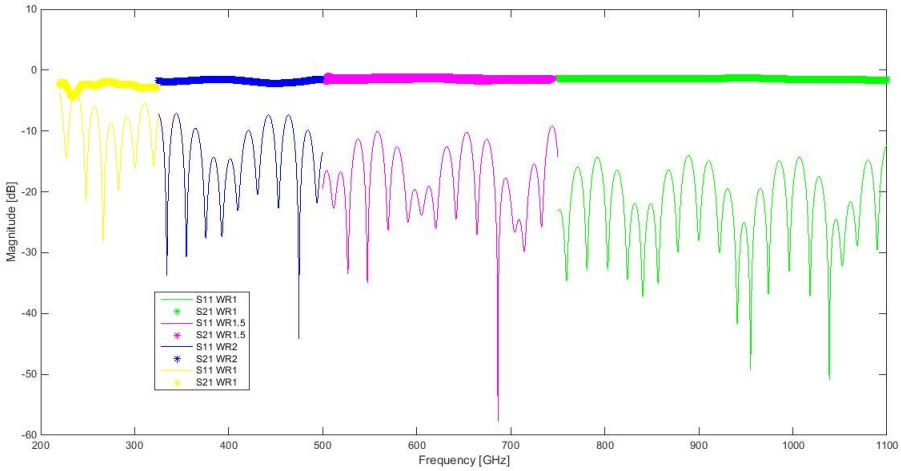

Figure 4.29: Different substrate thickness for the transition between CPW and PGL at different frequencies. 50 [μm] thickness (WR-03) at [220 - 325 GHz], 30 [μm] thickness (WR-02 and WR-1.5) at [325 - 500 GHz] and [500 - 750 GHz] and 20 [μm] thickness (WR-01) at [750 - 1100 GHz]

The results when the substrate is thinner are better, because as it can be seen in *Figure 4.29*, S_{11} is around -20 [dB] when the thickness is 20 [μm] and around -7 [dB] when the thickness is 50 [μm].

In *Figure 4.30* we also checked if a variation in the PGL width makes any difference, since for fabrication purposes probably it is better if the line is wider.

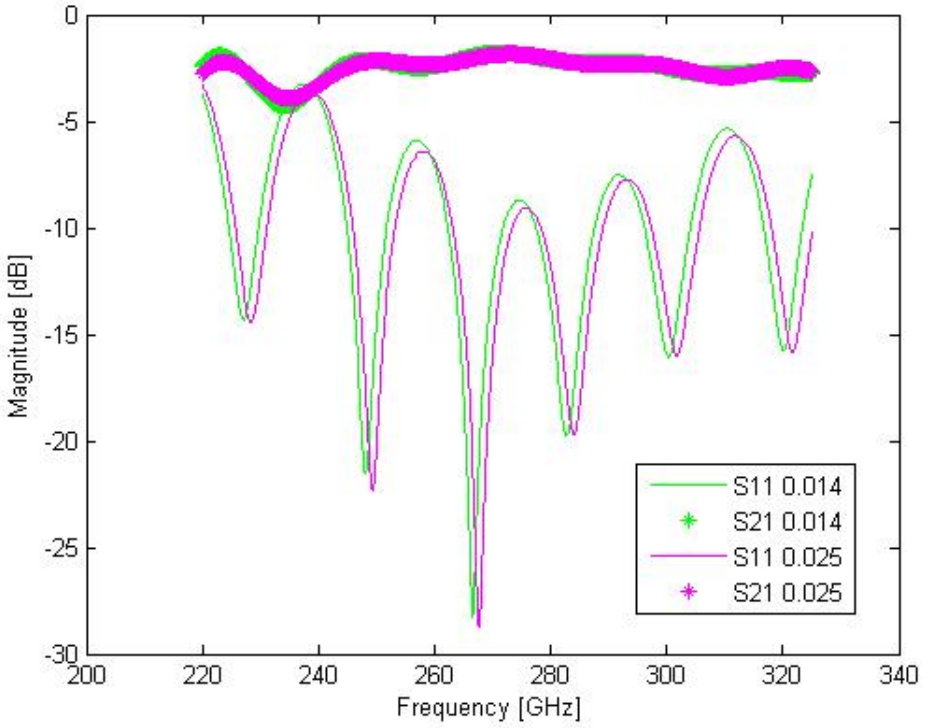

Figure 4.30: Different line width [mm] of PGL

Looking at the previous figure, *Figure 4.30*, it is obvious, that the PGL width does not affect to the transition performance.

During this chapter, the rules followed to get the complete model were explained, in the following one, the results for the complete model, as well as the difficulties found, will be analyzed.

5

Complete Sensor

Once that the different steps have been studied and used to optimize the parts of the proposed device separately, this Chapter will analyze the results obtained after put the two transitions together, that is, the transition between the rectangular waveguide and the CPW and the transition between the CPW and the PGL.
Moreover, during this chapter the difficulties found in the modeling process will be also analyzed.

220 - 325 [GHz] Sensor

In the previous chapter, we tested the differences between the performance with and without Via-Holes and it was seen how both results were similar. But it is also interesting to know what happens when the complete model has Via-Holes instead of walls, this fact can be seen in the following figure, *Figure 5.1*,

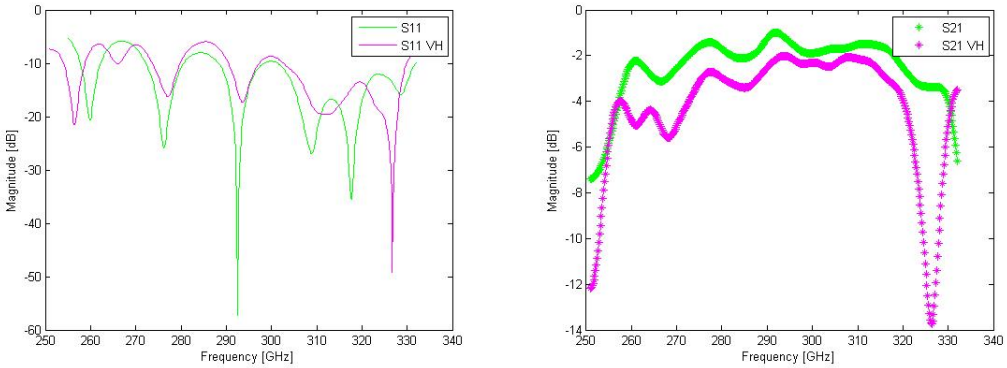

(a) Sensor S_{11} (b) Sensor S_{21}

Figure 5.1: S-Parameters results for the sensor at lower frequency with Walls and Via-Holes

The results with walls are better than the results with via holes, see *Figure 5.1*, with a variation of, approximately, 2 [dB].

From now on, the results just will be shown with walls, since they make the simulation more computing efficient.

325 - 500 [GHz] Sensor

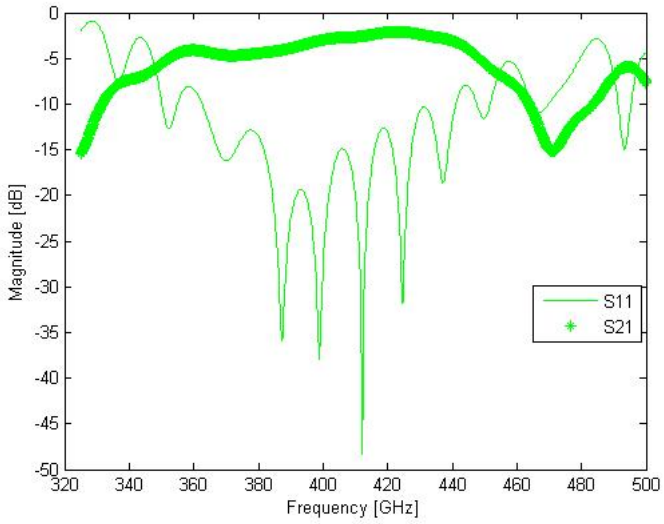

Figure 5.2: S-Parameters for the sensor with a frequency range between 325 and 500 [GHz]

At this frequency range, the bandwidth is between 390 and 440 [GHz], see *Figure 4.2.*Within the bandwidth, S-Parameters show that half of the power, is transmitted and not reflected, S_{11} is below -10 [dB] and S_{21} is around -3 [dB]. However, when frequency goes higher than 440 [GHz] the results become worse and worse, as it can be seen in the *Figures 5.3 and 5.4*

500 - 750 [GHz] Sensor

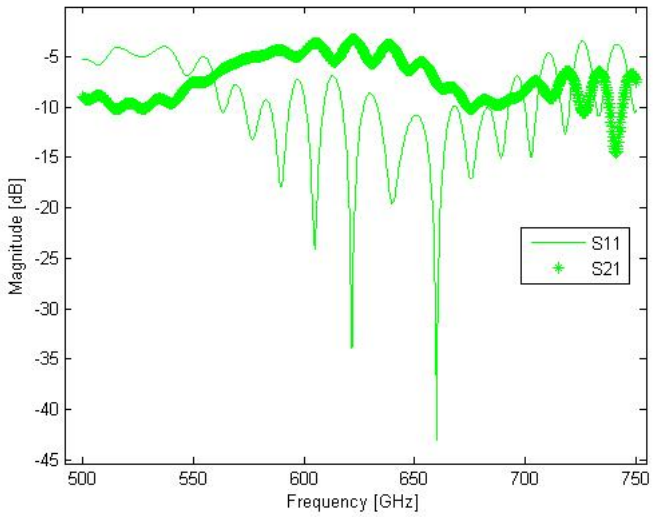

Figure 5.3: S-Parameters for the sensor with a frequency range between 500 and 750 [GHz]

750 - 1100 [GHz] Transition

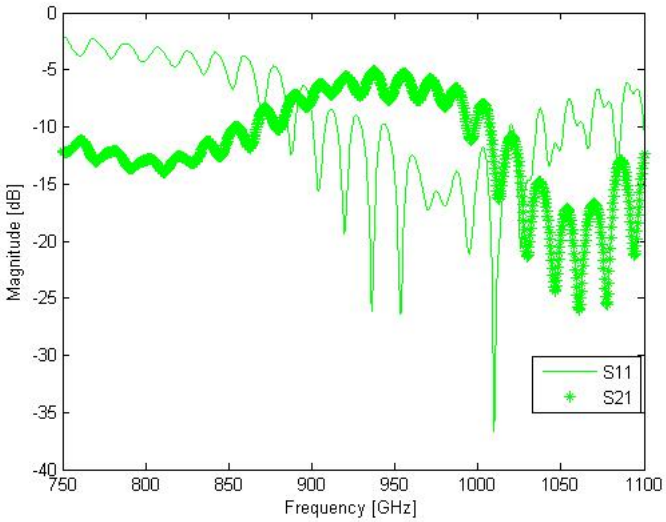

Figure 5.4: S-Parameters for the sensor with a frequency range between 750 and 1100 [GHz]

To figure out why the results for the highest frequencies are not as good as expected, a "De-Embedding" technique will be carried out. With this technique we will check how the S-Parameters look just after the first transition (WR-01+CPW), after adding the PGL, another CPW and the second WR-01, see *Figure 5.5*

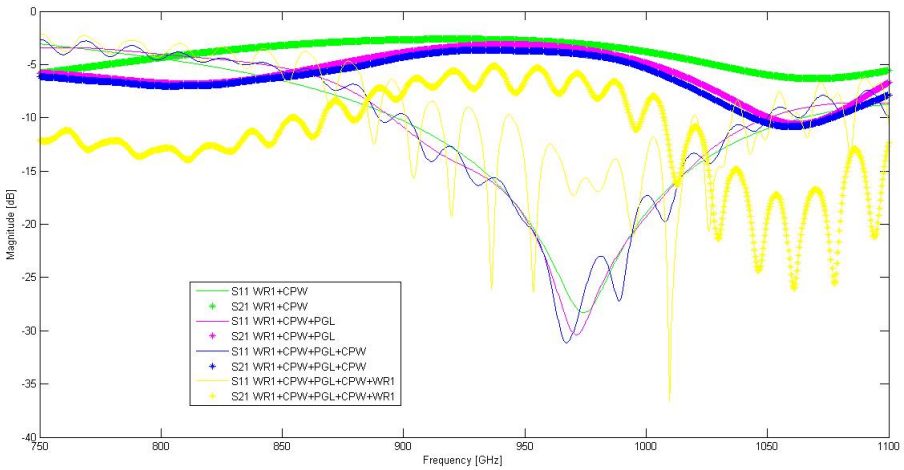

Figure 5.5: S-Parameters simulated in different reference planes to figure out which part make the results be not appropriate for our application.

Firstly, looking at *Figure 5.5* we can see how the results for the first transition, WR-01 to CPW (green line), are acceptable. Meaning, in the bandwidth between

800 - 1050 [GHz], S_{11} is below -10 [dB] and S_{21} is around -3 [dB]. After adding the PGL and the CPW, S_{21} falls until -5 [dB], i.e. more than half of the power is lost and the bandwidth also decreases. But it is in the moment when we add the second rectangular waveguide when the simulated results show that this designed device is not suitable for frequencies higher than 650 GHz.

In order to improve the results. The CPW was modified by increasing the length of its strip and changing the width of it, the strip can be seen in *Figure 4.18*, but it did not make any improving. The PGL was also modified making the line longer and smaller, but again, there was no better results for the complete sensor, see the PGL in *Figure 4.28*. So, we can conclude that for frequencies above 500 [GHz] the model starts working worse. This occurs because when the frequency increases more substrate modes affects the performance and also the radiations became more important.

In *Table 5.1* we can check how when the frequency is higher, the power lost by radiation and substrate modes [22] also increases.

	WR3	WR2	WR1.5	WR1
$\|S_{11}\|^2 + \|S_{21}\|^2$	0.65	0.49	0.4	0.31

Table 5.1: This table shows the increase of losses when the frequency increases. WR-03 works at [220 - 325 GHz], WR-02 at [325 - 500 GHz], WR-1.5 at [500 - 750 GHz] and WR-01 at [750 - 1100 GHz]

To finish this chapter, it is important to add a new issue that it was not taken into account previously, this issue is how affect material losses to the device performance.

5.0.1 Duroid and Losses

In this section we will study how losses, due to the dielectric substrate, affect to the device results. This study will be done just until 750 GHz, because for the highest range of frequencies the results are not adequate even without substrate losses.

The substrate material can be an important source of losses that affect the performance of the model. In Duroid 5880 datasheet [23], it can be seen that for 1 MHz the measured loss tagent is equal to 0.0004, and for 10 GHz is equal to 0.0009, as we do not know if the increase is linear with the frequency, we took 0.005 as a tagent loss for the whole frequency range between 220 and 750 GHz.

The obtained results are showed in the following figures, *Figure 5.6, 5.7 and 5.8*.

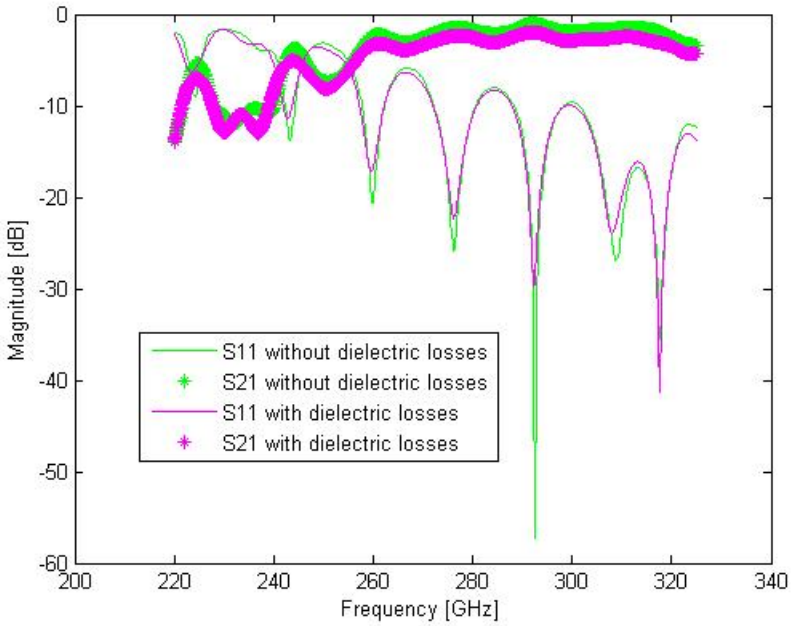

Figure 5.6: Sensor with and without dielectric losses for frequencies between 200 and 325 GHz. Tagent loss equal to 0.005

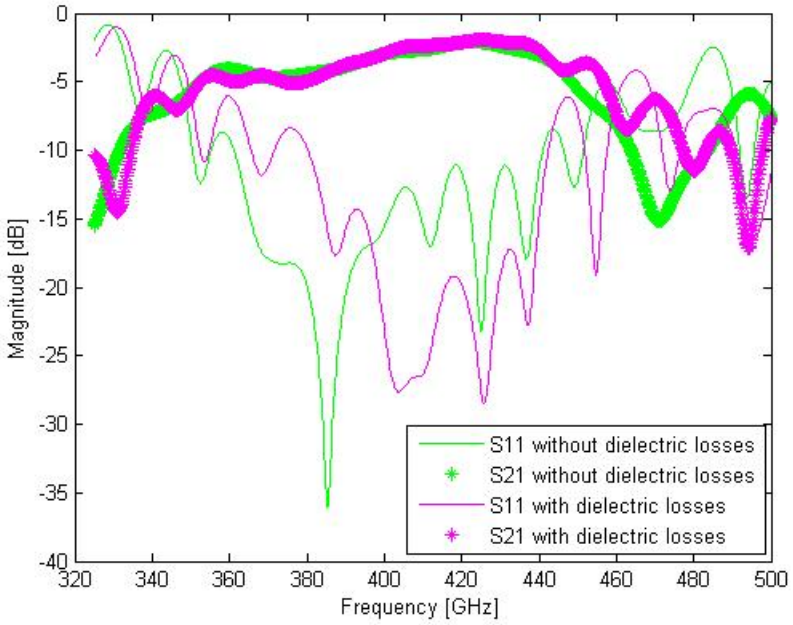

Figure 5.7: Sensor with and without dielectric losses for frequencies between 325 and 500 GHz. Tagent loss equal to 0.005

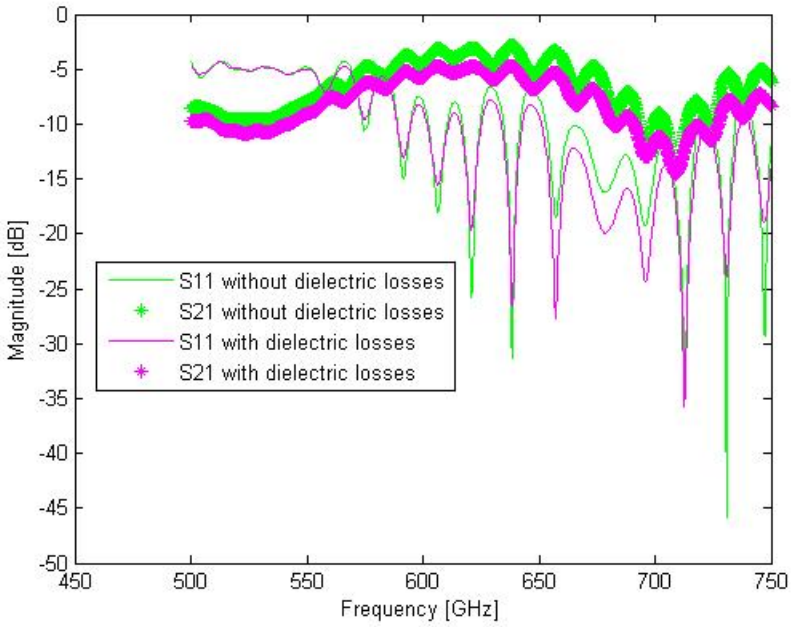

Figure 5.8: Sensor with and without dielectric losses for frequencies between 500 and 750 GHz. Tagent loss equal to 0.005

We also tried higher tagent losses to check when the sensor stop working and that value is equal to 0.03. With this value, S_{21} is lower than -5 [dB] within the bandwidth for each one of the frequency ranges.

6
Fabrication

During the development of this thesis, we also studied the possible fabrication problems that we could find in the fabrication process.

Substrate Material

The problem with the substrate is its weakness due to the thickness. That is why we need a metallic support under the substrate, but that support cannot be complete, since nor the CPW nor the PGL can have background. We would need an opening as the one showed in the *Figure 6.1*

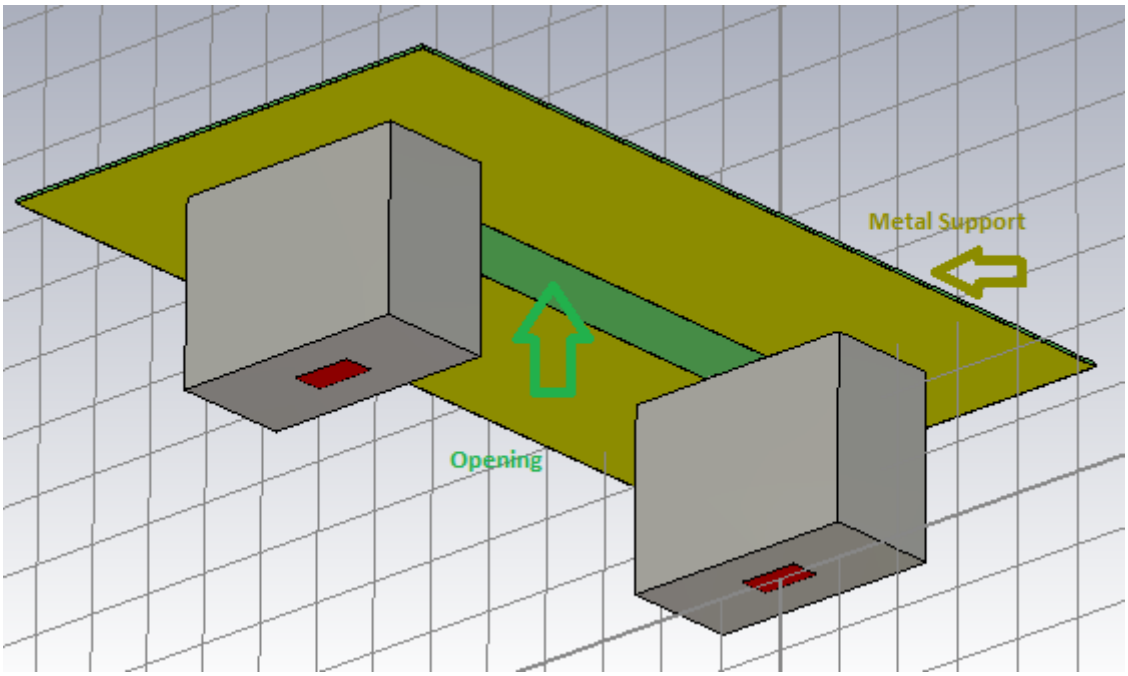

Figure 6.1: Sensor with metallic background

Drilling Via-Holes

Our worries about drilling were that our Via-Holes have a small diameter and the substrate where we have to make them is too thin. However, as it can be read in [28], there is no problem with drilling small Via-Holes in thin materials thanks to the new laser techniques in micromachining.

Tolerances

Looking at the *Figure 4.11*, we can observe the aperture of $\lambda/4$. In the fabrication part, this aperture is made by drilling, which means that probably the size is not going to be exact. That variation, see *Table 6.1*, decreases when the frequency increases, due to the rising of the sensitivity.

	WR-03	WR-02	WR-1.5	WR-01
Tolerance	± 40 µm	± 35 µm	± 30 µm	± 20 µm

Table 6.1: Tolerances for the aperture of $\lambda/4$

The tolerance results for Horizontal and Vertical Apertures can be checked in *Section 4.2.1 and 4.2.2* respectively.
About probe misalignment, it is a fact, that when frequency raises everything becomes more sensitive, so it seems obvious that the degree of freedom gets smaller.

7
Conclusion

The main goal in this thesis has been to develop a rectangular waveguide platform to avoid the use of probes, which provokes inaccuracy when several measurements are carried out. And to increase the range of working frequency until 1.1 THz.

Summarizing, this sensor is feed from a rectangular waveguide, the field going through the rectangular waveguide couples into the substrate reaching the CPW. And the CPW is the one that feeds the sensitive part of this sensor, the PLG.
Since the design process was too wide, it was carried out in different steps. The first one was to decide the material and thickness of the substrate, since using an inappropriate material can provoke that the sensor does not perform properly. Duroid is the best option, due to their low permittivity, 2.2, close to the air. Also we can conclude that a thin substrate works much better, due to the substrate modes that occur at sub-millimeter wave frequencies [22].

Once that the material and the substrate thickness were chosen, the following steps were the optimization of the first and second transition.

In the first transition (rectangular waveguide to CPW) the Horizontal and Vertical Apertures, the grounds of the CPW, the probes and the strip that goes from the probe to the CPW were optimized.

In the second transition (CPW to PGL) we tested different substrate thickness as well as the gobau line width.

After the optimizations, we simulated both transitions together. And from the results we can observe that when the frequency rises the working bandwidth decreases. Moreover, in the last two frequency ranges (from 500 - 1100 GHz) some resonances, due to the substrate modes and the radiations, appear deteriorating the results.

In the fabrication part, for each one of the range frequencies some tolerances have to be taken into account, they are described in *Chapter 6* with other fabrication issues.

Thanks to the robustness of the model and the huge range of frequencies in which it works, lots of accurate measurements of bio-material will be taken, helping to the research growth of this field.

Bibliography

[1] James C. Wiltse. History of Millimeter and Submillimeter Waves. IEEE Transactions on Microwave Theory and Techniques, Vol. MTT-32, No. 9, September 1984.

[2] Peter H. Siegel, Fellow IEEE. Terahertz Technology in Biology and Medicine. California Institute of Technology, Pasadena, CA, 91125.

[3] Gerald J. Wilmink Jessica E. Grundt. Invited Review Article: Current State of Research on Biological Effects of Terahertz Radiation. J Infrared Milli Terahz Waves (2011) 32:1074–1122.

[4] Peter H. Siegel, Fellow, IEEE. Terahertz Technology. IEEE TRANSACTIONS ON MICROWAVE THEORY AND TECHNIQUES, VOL. 50, NO. 3, MARCH 2002.

[5] Microwave Engineering, David M. Pozar.

[6] Foundations for Microwave Engineering, E. Collin.

[7] ROBERT W. JACKSON, MEMBER, IEEE. Considerations in the Use of Coplanar Waveguide For Millimeter-Wave Integrated Circuits. IEEE TRANSACTIONS ON MICROWAVE THEORY AND TECHNIQUES, VOL. MTT-34, NO. 12, DECEMBER 1986

[8] John Coonrod Rogers Corp., Chandler, AZ Brian Rautio Sonnet Software Inc., North Syracuse, NY. Comparing Microstrip and CPW Performance. Microwave Journal, Vol. 55, No. 7, July 2012.

[9] A. Treizebre and B. Bocquet. Nanometric metal wire as a guide for THz investigation of living cells. Int. J. Nanotechnol., Vol. 5, Nos. 6/7/8, 2008.

[10] Johanna Hanning. Characterisation of terahertz integrated membrane circuits, 2015.

[11] Daniel Sanchez-Escuderos, Miguel Ferrando-Bataller, Mariano Baquero-Escudero, Antonio Berenguer. Leaky-Wave Antenna on Planar Goubau Line at THz Frequencies. 2013, 7th European Conference on Antennas and Propagation (EuCAP)

[12] GABRIEL M. REBEIZ, MEMBER, IEEE, Millimeter-Wave and Terahertz Integrated Circuit Antennas.

[13] Gabriel M. Rebeiz, Member IEEE, Dayalan P. Kasilingam, Member IEEE, Yong Guo, Philip A. Stimson and David B. Rutledge, Senior Member IEEE. Monolithic Millimeter-Wave Two-Dimensional Horn Imaging Arrays. IEEE Transactions On Antennas and Propagation, Vol. 38, No. 9, September 1990.

[14] W. Che, K. Deng, D. Wang and Y.L. Chow. Analytical equivalence between substrate-integrated waveguide and rectangular waveguide.

[15] Ke Lu, Member, IEEE. An Efficient Method for Analysis of Arbitrary Nonuniform Transmission Lines. IEEE TRANSACTIONS ON MICROWAVE THEORY AND TECHNIQUES, VOL. 45, NO. 1, JANUARY 1997.
[16] Farzaneh Taringou and Jens Bornemann. New Substrate-Integrated to Coplanar Waveguide Transition. Proceedings of the 41st European Microwave Conference.
[17] Dominic Deslandes and Ke Wu. Integrated Transition of Coplanar to Rectangular Waveguides. Poly-Grames Research Center, Ecole Polytechnique de Montreal, C.P. 6079, Succ. Centre Ville, Montreal, QuCbec, H3C 3A7, Canada.
[18] Dominic Deslandes.Design Equations for Tapered Microstrip-to-Substrate Integrated Waveguide Transitions. Department of Computer Science, Universite du Quebec a Montreal, Montreal, Quebec, H2X 3Y7, Canada.
[19] Lin Li, Xiaoping Chen, Roni Khazaka, Ke Wu. A Transition from Substrate Integrated Waveguide (SIW) to Rectangular Waveguide.
[20] Teng Li, Hongfu Meng and Wenbin Dou. Broadband transition between substrate interated waveguide and rectangular waveguide based on ridged steps. IEICE Electronics Express, Vol. 11, No. 13, 1-7.
[21] Kazuyuki Seo. Planar Microstrip-To-Waveguide Transition in Millimeter-Wave Band. Chapter 11.
[22] R.J.Collier. COUPLING BETWEEN COPLANAR WAVEGUIDES AND SUBSTRATE MODES. The Electronic Engineering Laboratory, The University, Canterbury, Kent, U.K. CT2 7NT.
[23] RT/duroid® 5870 /5880 High Frequency Laminates. Rogers Corporation.
[24] Feng Xu and Ke Wu, Fellow, IEEE. Guided-Wave and Leakage Characteristics of Substrate Integrated Waveguide. IEEE TRANSACTIONS ON MICROWAVE THEORY AND TECHNIQUES, VOL. 53, NO. 1, JANUARY 2005.
[25] Dominic Deslandes, Member, IEEE, and Ke Wu, Fellow, IEEE. Accurate Modeling, Wave Mechanisms, and Design Considerations of a Substrate Integrated Waveguide. IEEE TRANSACTIONS ON MICROWAVE THEORY AND TECHNIQUES, VOL. 54, NO. 6, JUNE 2006.
[26] Via Hole Design Guidelines. Ion Beam Milling, Inc.
[27] Anthony Treizebré, Tahsin Akalin, and Bertrand Bocquet. Planar Excitation of Goubau Transmission Lines for THz BioMEMS. IEEE MICROWAVE AND WIRELESS COMPONENTS LETTERS, VOL. 15, NO. 12, DECEMBER 2005.
[28] Laser Hole Drilling. laserod.com
[29] Tom Lee. Bridging the Terahertz Gap: Progress and Challenges. Stanford University, Dept. of Electrical Engineering, Stanford, CA 94305 USA.
[30] http://www.teraphysics.com/understanding-thz.php
[31] Fundamentals of Vector Network Analysis. Rohde Schwarz.
[32] Rectangular Waveguide. http://cc.ee.ntu.edu.tw/ jfkiang/electromagnetic

A

Appendix I

At the beginning of this thesis we considered different approaches to supress on-probe measurements, until we figure out which one was the best option for us.

A.1 Antennas

As first approach we thought in Antennas[11], as way to feed the PGL, due to their resistance to substrate modes when they are integrated on thin dielectric membranes [12][13]. These *substrate modes* are one of the main problems for the device performance at high frequencies. Since the relative permittivity of the substrate depends on the frequency, when that frequency is too high, these modes make the energy not couple provoking losses.
We need a design based on waveguide connections to the VNA, so, the problem came when we tried to figure out how to illuminate the antenna and test the results. This fact, seemed to challenge, and we decided to think in another possible solution. Since, for us, it is important to be able to feed and test the device through common rectangular waveguides. Using rectangular waveguides as a part of our model is essential, moreover it makes the device more compact and robust.
Thinking in that, we arrived to the following approach based on a type of waveguide called Substrate Integrated Waveguide (SIW).

A.2 Substrate Integrated Waveguide

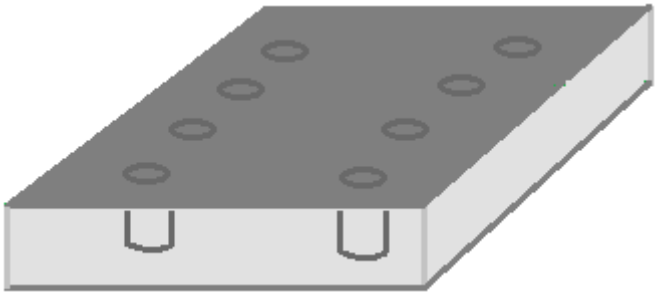

Figure A.1: Substrate Integrated Waveguide

Substrate Integrated Waveguide (SIW) technology is being used more and more thanks to its planar form , as it can be seen in *Figure B*.1, which make it more

appropriate to connect with other planar structures on the same substrate, i.e. microstrip or CPW for example[16][17][18].
SIW are planar structures with two rows of metallic via-holes in opposite sides of the waveguide, which are used to connect the parallel metal plates *Figure 3.1.* This waveguide is completely compatible with the classical rectangular waveguide [14], and also has the same propagation characteristics, that is why there is no problem in using SIW instead of common rectangular waveguides.
For our approximation, two SIWs, two microstrip and a PGL were used. In order to match the SIWs to the PGL the calculations showed in [15] were taken into account. In next figure can be seen how the final model using this technology looks .

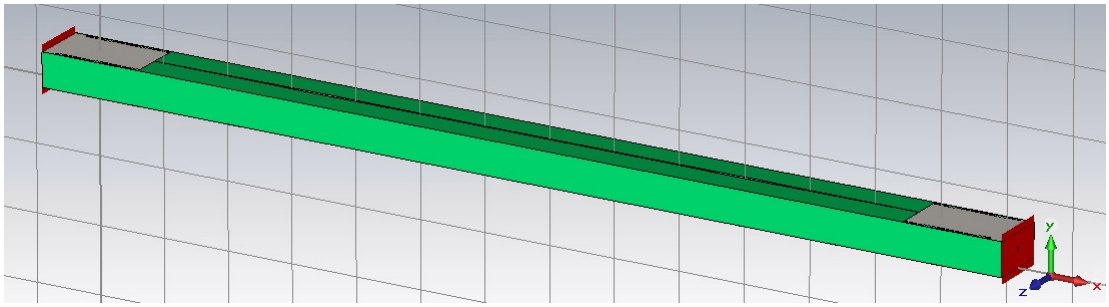

Figure A.2: Complete model using SIW

For checking how efficient this model is, we can look at the S-Parameters in *Figure* 3.3,

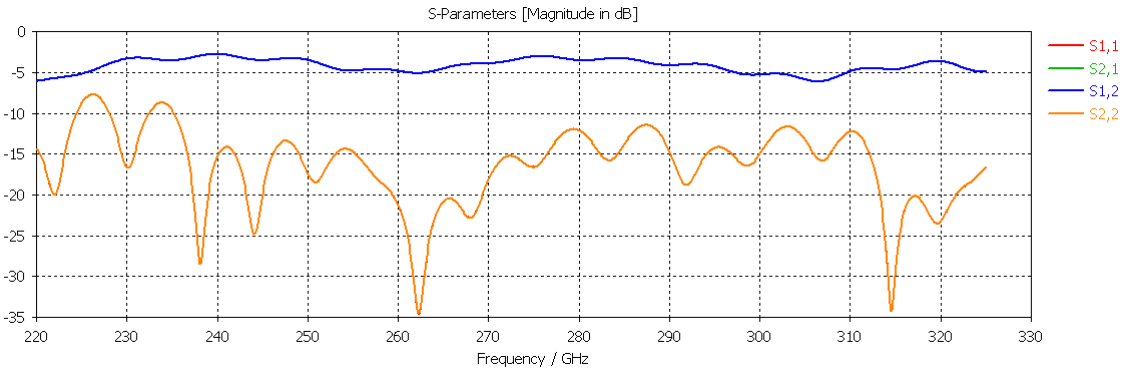

Figure A.3: S-Parameters

The fact that S_{ii} are below -10 [dB], and the S_{ji} and the S_{ij} around -3 and above -5 [dB] show that half of the energy is being transmitted and not reflected. S_{ji} and S_{ij} are not 0 [dB] mainly because of the substrate modes and radiations, which are the basic problems of this frequencies.
Until this point, the proposed model seemed a good approximation to reach our goal, but the problem came when we thought in how to feed the SIWs.
As it was already said, for us, the easiest way to feed the sensors is by using regular rectangular waveguides. So, we tried to figure out how to connect the SIWs to a common rectangular waveguide, some studies have done some research about this

issue [19][20]. The frequencies that they are using there are much lower than ours, and it is a fact that when frequency raises, devices sizes decrease. So, it was by then when we realised how small was that transition going to be. For example, in a transition based on ridged steps, as in [20], these steps could not be thicker than 86 [μm] for the lowest range of frequencies, or 25 [μm] for the highest, which would make the construction difficult. That is why we had to stop and think in another option more suitable to construct and test.